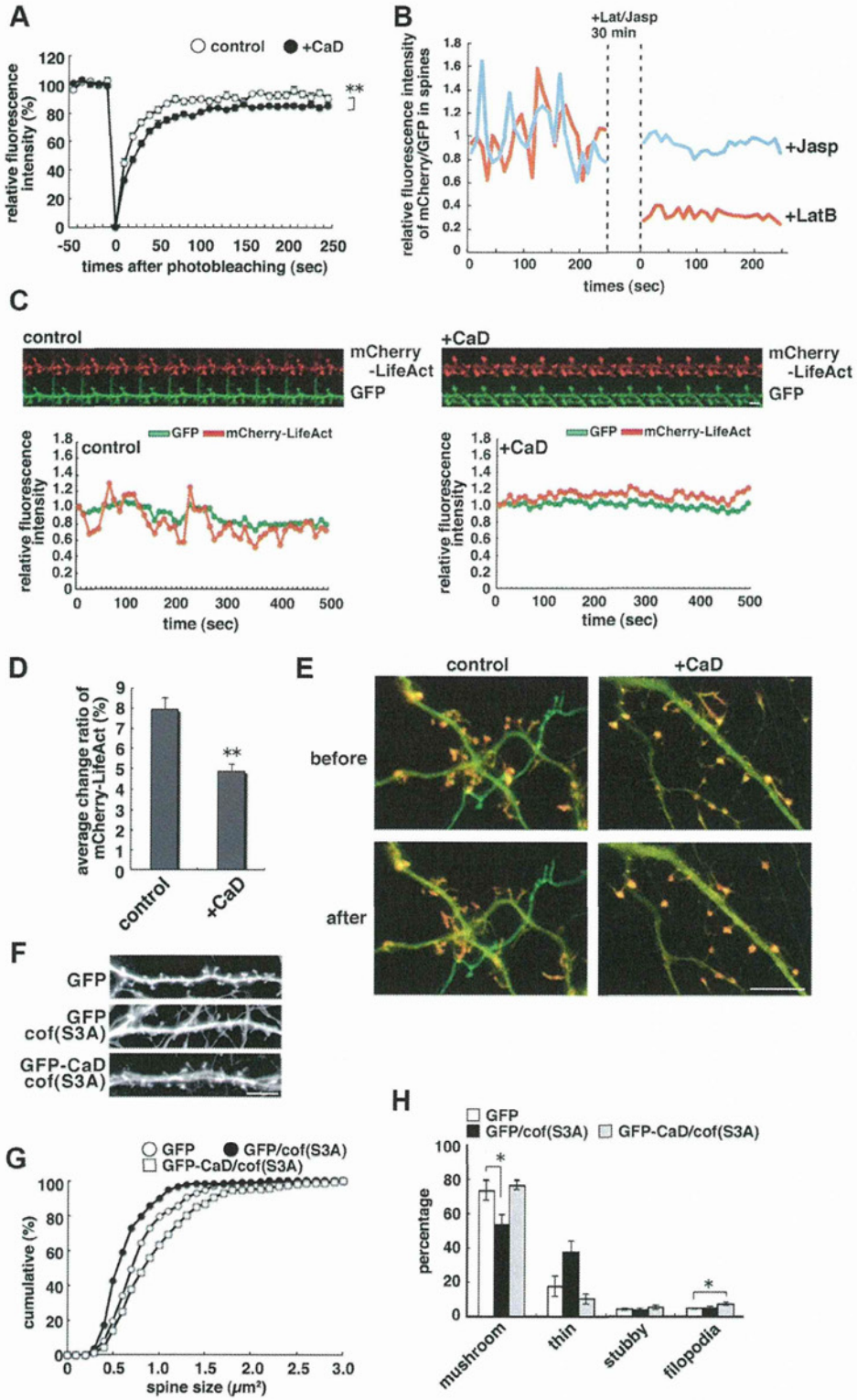

Figure 3. CaD effect on actin dynamics. ***A***, The fluorescence recovery of mCherry-β-actin over time after photobleaching, measured in neurons transfected with a mock vector (control) or myc-tagged-CaD (+CaD). Data are means ± SE of values from 10 cells (**$p < 0.01$). ***B***, Hippocampal neurons were transfected with GFP and mCherry-LifeAct to visualize spine volume changes and F-actin dynamics. The neurons were treated with Jasp or LatB for 30 min in the middle of the observation period, and changes in the mCherry and GFP fluorescence intensities in the spines were measured. The graph shows F-actin dynamics, corrected for the spine volume change (mCherry/GFP). F-actin dynamics were suppressed at high Jasp or low LatB levels; these agents elicit F-actin stabilization and depolymerization, respectively. ***C***, Neurons were transfected with GFP, mCherry-LifeAct, and either a mock vector (control) or myc-CaD (+CaD). Changes in fluorescence intensities in spines, observed every 10 s (top) (scale bar, 2 μm), are shown in the graph (bottom). Compared with GFP intensity changes, the mCherry intensity fluctuated dramatically in control neurons, whereas both the GFP and mCherry intensities were relatively stable in CaD-transfected neurons. ***D***, Spine F-actin dynamics, observed with mCherry-LifeAct. The graph shows change rates of mCherry-LifeAct fluorescence intensity in spines. Data are means ± SE of values from at least 18 spines (**$p < 0.01$). ***E***, Neurons were transfected with GFP and mCherry-LifeAct to visualize the spine shape and the F-actin activity, and F-actin accumulation in spines was observed before or after LatB treatment. Scale bar, 10 μm. ***F***, Spine morphology in neurons transfected (*Figure legend continues.*)

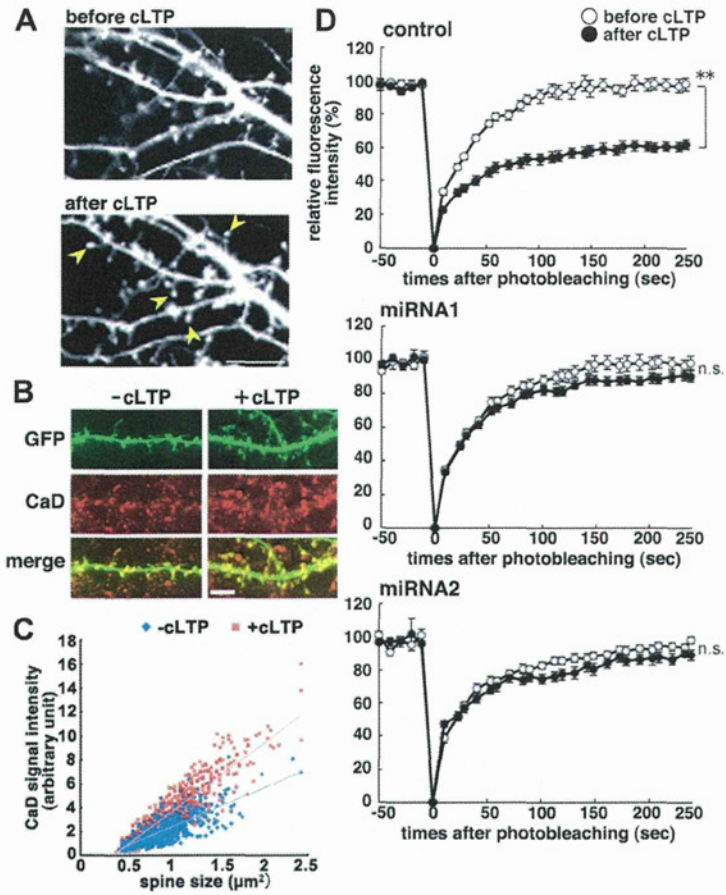

Figure 4. CaD is necessary for chemical LTP to induce F-actin stabilization in spines. ***A***, Spine morphology before and after cLTP; yellow arrowheads indicate enlarged spines after cLTP (scale bar, 10 μm). ***B***, CaD accumulation in enlarged spines after cLTP (scale bar, 5 μm). ***C***, Scatter plot of spine sizes versus CaD intensities in each spine in neurons with (red square) or without cLTP (blue diamond). Data are obtained from at least 727 spines ($p < 0.01$). ***D***, Fluorescence recovery of mCherry-β-actin over time after photobleaching, in hippocampal neurons transfected with control miRNA, CaD miRNA1, or CaD miRNA2. FRAP assays were performed before and after cLTP. Data are means ± SE of values from at least 10 cells (**$p < 0.01$).

least three times independently. Statistical significance was evaluated by classical Student's *t* test, paired *t* test, or one-way ANOVA.

Results

CaD accumulates in spines

CaD levels increased during development of rat hippocampal neurons in culture and reached a peak at 16–21 d *in vitro* (DIV), concurrent with dramatic increases in the postsynaptic protein PSD-95 and the presynaptic protein synapsin I (Fig. 1*A*). GFP-tagged full-length CaD (GFP-CaD) exogenously expressed in the neurons appeared to accumulate in spines (Fig. 1*B*). The CaD (GFP-C-CaD) C-terminal fragment, which includes actin-binding domains, was also localized to spines, while the N-terminal fragment (GFP-N-CaD), which lacks actin-binding ability, was dispersed through both dendrites and spines (Fig. 1*B*,*C*). These results suggest that CaD accumulates in spines by associating with F-actin via its actin-binding domains. Consistent with this scenario, endogenous CaD was localized in the spines and was resistant to Triton X-100 treatment (Fig. 1*D*, left). The Triton X-100 resistance was abolished by the F-actin-depolymerizing agent latrunculin B (LatB) (Fig. 1*D*, right). In sedimentation assays, ~60% of the CaD protein cosedimented with β-actin in the Triton X-100-insoluble fraction, and LatB treatment shifted their localization to the soluble fraction (Fig. 1*E*). After treatment with the actin-polymerizing agent jasplakinolide (Jasp), >80% of the CaD and β-actin cosedimented in the insoluble fraction (Fig. 1*E*). Fluorescence recovery after photobleaching (FRAP) assay also revealed that Jasp treatment reduced the GFP-CaD turnover rate in spines (Fig. 1*F*). These data demonstrate that CaD is actively accumulated into spines through its association with F-actin.

CaD enlarges the spine heads by stabilizing actin filaments

To determine the function of CaD in spine dynamics, we overexpressed the CaD fragments in neurons. While GFP-CaD or GFP-C-CaD induced larger spine heads than GFP did alone, GFP-N-CaD did not (Fig. 2*A–C*). We also depleted endogenous CaD using plasmid-type miRNA expression vectors, which were validated in previous studies (Fukumoto et al., 2009; Morita et al., 2012). Depleting endogenous CaD markedly reduced the spine-head size and changed the spine shape from mushroom to thin or filopodial (Fig. 2*D–F*). FRAP assay using mCherry-β-actin revealed that exogenous CaD significantly reduced the actin turnover rate within spines (Fig. 3*A*). The time constants (inverse of the turnover rate) for actin turnover were 19.3 ± 1.1 s in GFP-transfected neurons versus 24.6 ± 0.9 s in GFP-CaD-transfected neurons ($p < 0.01$). These data indicated that F-actin was stabilized. We also measured F-actin dynamics using mCherry-LifeAct, which selectively binds to F-actin and demonstrated real-time changes in the amount of F-actin within spines (Fig. 3*B*). The dendritic spines exhibit spontaneous motility as previously reported (Fischer et al., 1998, 2000; Korkotian and Segal, 2001; Star et al., 2002), and the dynamic motility is crucially based on the actin cytoskeleton (Fischer et al., 1998; Star et al., 2002). In control neurons, the amount of F-actin in spines varied dramatically compared with the spine volume traced by GFP (Fig. 3*C*). F-actin localization in CaD-transfected spines was more stable than that in control spines (Fig. 3*C*,*D*). This localization was resistant to LatB treatment (Fig. 3*E*), implicating that CaD stabilizes F-actin turnover in spines. Cofilin is considered to be a main factor for F-actin depolymerization and severing in spines (Lisman, 2003; Sarmiere and Bamburg, 2004). Indeed, cof(3A) (constitutively active cofilin) reduced the spine-head size (Fig. 3*F*,*G*). Interestingly, GFP-CaD protected F-actin from cof(3A) attack and thus promoted mushroom-shaped spines (Fig. 3*F–H*). Together, these results indicate that CaD stabilizes actin filaments in spines, leading to larger spine heads.

←

(*Figure legend continued.*) with GFP, GFP-CaD, and/or cof(S3A) (scale bar, 10 μm); the graph shows spine sizes and their cumulative distributions (***G***) and classification of spine morphology (***H***). Dendritic protrusions in the neurons were classified by morphology: mushroom, thin, stubby, or filopodial. Data are means ± SE of values from at least 147 spines.

CaD is necessary for chemical LTP to induce F-actin stabilization in spines

Actin filament stabilization is tightly linked to LTP-induced spine-head enlargement (Lisman, 2003; Hotulainen and Hoogenraad). In cultured hippocampal neurons, cLTP triggered to enlarge spine heads (Fig. 4*A*) and to accumulate endogenous CaD into the enlarged spine heads (Fig. 4*B*,*C*), suggesting that accumulated CaD contributes to stabilizing actin filament in the spines. FRAP assay confirmed that cLTP-induced spine head enlargement was associated with F-actin stabilization (Fig. 4*A*,*D*). In CaD-knockdown neurons, however, cLTP treatment did not stabilize F-actin (Fig. 4*D*). These results strongly suggest that CaD is critical for cLTP-induced F-actin stabilization in spine head enlargement.

CORT decreases CaD expression levels

We previously identified that CaD is one of the main downstream molecules in the GC-induced detrimental effects on the radial migration of neural progenitor cells during neocortical development (Fukumoto et al., 2009). Numerous studies have reported stress-induced increase in GC concentrations in the blood plasma or serum. However, GC concentration in the brain under nonstressed and stressed conditions remained unclear. Under conventional culture conditions without serum, neurons are, therefore, cultured in medium containing GC at nonstressed blood concentrations. To examine how GCs affect dendritic spine formation in cultured hippocampal neurons, we first examined the concentration of corticosterone (CORT), the principal GC in many species including rodents, in rat blood plasma and brain extracts after foot-shock stress. The CORT concentration increased markedly after stress, from 77.9 ± 30.0 nM to 1577.8 ± 191.6 nM ($p < 0.01$) in the blood plasma and from 16.7 ± 0.5 nM to 275.0 ± 36.0 nM ($p < 0.01$) in the brain (Fig. 5*A*). To culture hippocampal neurons with these CORT concentrations, our culture medium was prepared using CORT-free B27 supplement, with CORT added to defined concentrations. Importantly, the CaD levels decreased markedly according to the CORT dosage (Fig. 5*B–E*), and the F-actin was simultaneously decreased in spines (Fig. 5*D*, bottom). Thus, these results suggest that chronic CORT treatment decreases the localization of F-actin as well as CaD in spines, leading to the reduction of spine head size.

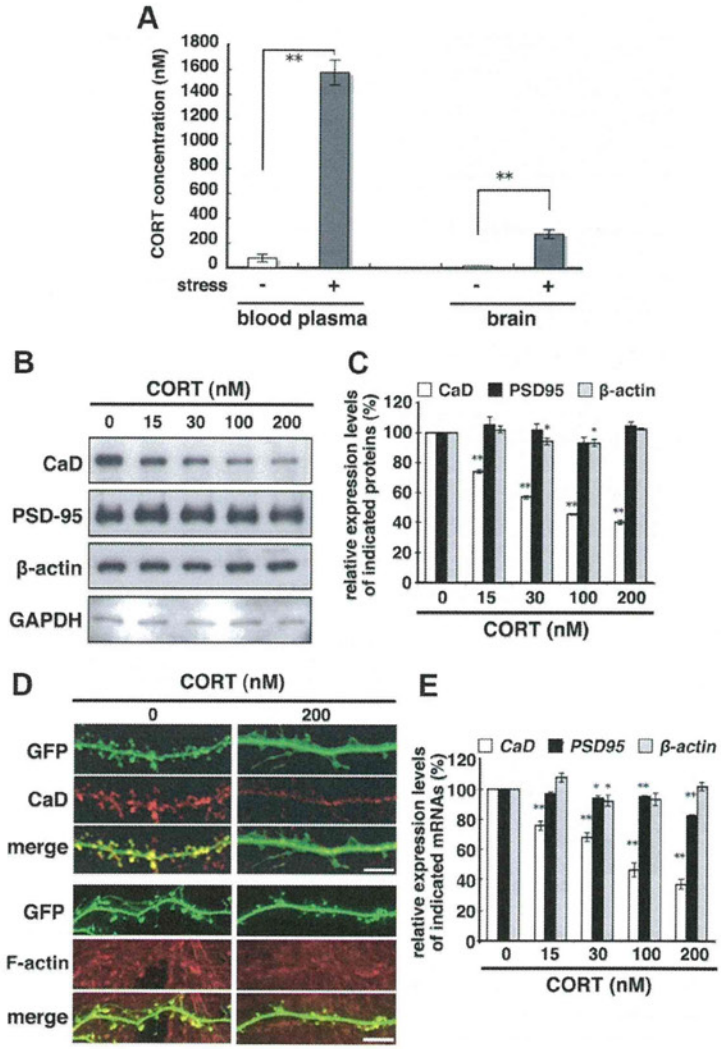

Figure 5. CORT decreases CaD expression. ***A***, A graph of CORT concentrations in blood plasma and brain extract; stress-induced CORT concentrations were measured shortly after rats received four uncontrollable, inescapable foot shocks. Data are means ± SE of values from three independent experiments (**$p < 0.01$). ***B***, CORT dose-dependent effects on CaD, PSD-95, and β-actin protein levels in neurons. Neurons were cultured with the indicated concentrations of CORT throughout the culture and prepared samples at 21–24 DIV. ***C***, Immunoblots shown in ***B*** were quantified by densitometry. Data are means ± SE of values from three independent experiments (*$p < 0.05$, **$p < 0.01$). ***D***, GFP-transfected neurons cultured with 0 or 200 nM CORT were fixed and stained with anti-GFP and anti-CaD antibodies (scale bar, 10 μm). ***E***, CORT dose-dependent effects on *CaD*, *PSD-95*, and β-actin mRNA levels, determined by RT-PCR. Data are means ± SE of values from three independent experiments (*$p < 0.05$, **$p < 0.01$).

We previously reported that the CaD gene encodes multiple isoforms, and that the fibro- and HeLa-type promoter regions, which function independently, regulate their transcription (Yano et al., 1994). In hippocampal neurons, CORT treatment suppressed the fibro-type isoforms more severely than the HeLa-type isoforms (Fig. 6*A*). Reporter assays showed that CORT reduced the CaD fibro-type promoter activity (Fig. 6*B*). The CaD promoter contains two putative *cis*-elements: a serum response factor (SRF)-binding CArG-box and a positive glucocorticoid receptor (GR)-binding glucocorticoid-responsive element (GRE)-like sequence (Mayanagi et al., 2008). In hippocampal neurons, the positive GRE-like sequence was not involved in CaD promoter activity, whereas a CArG-box mutation reduced the CaD promoter basal activity; CORT treatment did not produce any additional effect on this activity (Fig. 6*B*). These results suggest that CaD transcription was promoted by the SRF/CArG-box and was reduced by CORT through inhibition of the SRF/CArG-box-dependent transcription.

CORT prevents spine development by downregulating CaD

Consistent with the decrease in CaD and F-actin contents, CORT treatment resulted in smaller spine heads and a larger proportion of thin spines. At CORT levels of 100–200 nM, as found in the rat

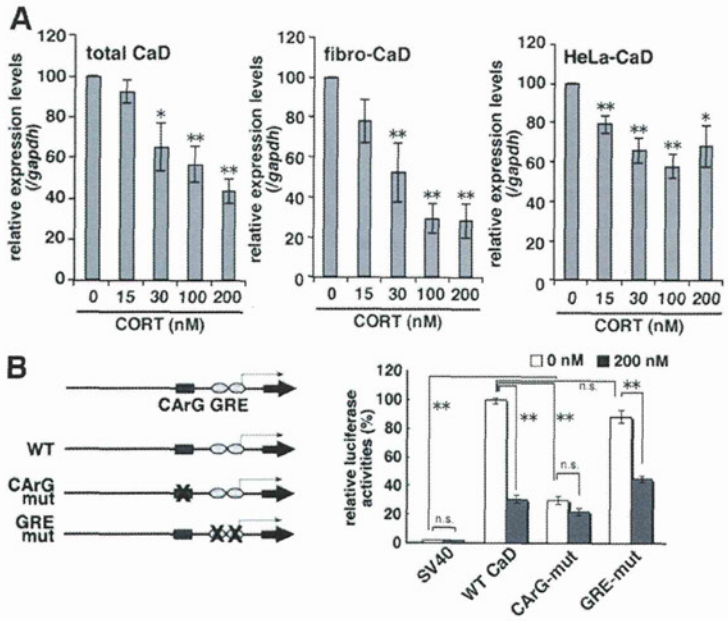

Figure 6. CORT effects on CaD isoform levels. ***A***, Hippocampal neurons were cultured with CORT at the indicated concentrations. Total RNA was extracted, and RT-PCR was performed using specific primers for total CaD, fibro-type CaD, and HeLa-type CaD. Data are means ± SE of values from five independent experiments (*$p < 0.05$, **$p < 0.01$). ***B***, A schematic diagram of mutation constructs of the CArG-box or GRE-like sequences in the rat fibro-type CaD promoter. Reporter assays were performed in hippocampal neurons (21–23 DIV) cultured with 0 or 200 nM CORT using the indicated promoter constructs. Reporter plasmid containing SV40 promoter (pGL3promoter) was used as a control. Data are means ± SE of values from three independent experiments (**$p < 0.01$).

brain under stress conditions, thin spines predominated with a corresponding decrease in the number of mushroom spines (Fig. 7*A–C*). FRAP assay demonstrated that CORT increased actin turnover rate (Fig. 7*D*). The time constants for actin turnover were 19.1 ± 0.7 s in the neurons cultured with 200 nM CORT compared with 28.6 ± 0.6 s in those cultured without CORT ($p < 0.01$). LifeAct assay also showed that CORT reduced the spine F-actin stability (Fig. 7*E*). As many actin-regulating proteins have been reported to modify spine shape, head size, and function (Lisman, 2003), we used RT-PCR to examine the expression of 25 actin-regulating genes. While CORT treatment affected the expression of some of these genes to a degree (data not shown), only CaD expression was markedly decreased (Fig. 5*B–E*). To confirm the importance of CaD reduction in the detrimental effect of CORT on dendritic spine development, we overexpressed CaD under high CORT concentrations. Exogenous CaD enlarged the spine-head size and promoted mushroom-shape spines even in the presence of 200 nM CORT (Fig. 8*A–C*). The spine F-actin stability that was reduced by CORT treatment was recovered by exogenous CaD (Fig. 8*D*,*E*). Both FRAP and LifeAct assays showed that exogenous CaD stabilized F-actin even under 200 nM CORT treatment [time constants in FRAP for CORT-treated spines: 17.8 ± 0.9 s vs for GFP-CaD-transfected CORT-treated spines: 28.0 ± 0.8 s ($p < 0.01$)]. These results suggest that CaD is a critical downstream player in the detrimental effects of CORT on actin cytoskeleton-dependent development of dendritic spines.

Discussion

In this study, we demonstrated that CaD modulates the spine-head size in cultured hippocampal neurons by regulating F-actin dynamics. CaD inhibits actin-myosin interactions and potently stabilizes F-actin (Sobue and Sellers, 1991; Mayanagi and Sobue, 2011). In hippocampal neurons, CaD was accumulated in spines via an interaction with F-actin (Fig. 1*B*), indicating that the function of CaD in spines depends on actin. Both full-length CaD and the CaD C-terminal fragment stabilized F-actin and increased the spine-head size (Fig. 2). Chemical LTP induction requires reorganization of the actin cytoskeleton, which shifts the G/F-actin ratio toward stable F-actin and increases the spine-head size (Gu et al., 2010). CaD was accumulated in spine heads in response to cLTP and stabilized the actin dynamics (Fig. 4). These results indicated that CaD was integral to this actin reorganization in spines (Figs. 2–4). Thus, F-actin dynamics regulated by CaD is critically involved in spine development and plasticity. Because CaD localization at spine heads also depends on F-actin, cooperative bidirectional interactions between CaD and F-actin may be ultimately required for regulating spine stability.

Neuronal architectures such as dendritic arborization and synaptic structure have plasticity in response to various factors, and this structural remodeling occurs throughout the lifespan (Dumitriu et al., 2010; McEwen, 2010; Liston and Gan, 2011; Bloss et al., 2011). These alterations correlate with cognitive and behavioral functions (Dumitriu et al., 2010; Bloss et al., 2011). Although transient stress exposure evokes adaptive responses of the hypothalamus-pituitary-adrenal (HPA)-axis, repeated or chronic stress causes the hyperactivation of this cascade. GCs have been intensely studied as a principal stress mediator. Exposure to high GCs triggers adverse effects on synapse formation, dendritic arborization, and hippocampal volume (Watanabe et al., 1992; Magariños et al., 1996; McEwen, 1999, 2005; Wellman, 2001; Radley et al., 2004; Radley et al., 2006; Liston and Gan, 2011). However, the molecular mechanisms are not fully understood. To examine the effects of GCs on cultured hippocampal neurons, we first measured the actual CORT concentrations in the blood plasma and brain of rats with or without foot-shock stress. Unexpectedly, the CORT concentrations in the brain were fivefold lower than those in the blood plasma, but they increased 16-fold after foot-shock stress (Fig. 5*A*). To test the effect of CORT levels on hippocampal neurons, we used a culture medium with a CORT-free B27 supplement and added CORT to defined concentrations. Using this culture system, we demonstrated that CORT at physiological concentrations inhibited dendritic spine development (Fig. 7*A–C*). F-actin dynamics are strongly linked to spine shape, motility, and plasticity (Hotulainen and Hoogenraad, 2010). CORT treatment destabilized the spine F-actin dynamics, changing the spine morphology from a mature mushroom shape to premature, thin, and filopodial shapes, as well as decreasing the spine-head size (Fig. 7). These data provide a novel insight regarding CORT-induced spine shrinkage as well as suppression of synapse formation and maturation. Previous *in vivo* histological studies have shown that chronic stress exposure decrease the number of dendritic spines (Radley et al., 2006). In addition, Liston and Gan

(2011) have recently reported that in the living cortex, CORT exposure leads to the loss of stable, mature spines with increasing filopodial and thin spines and spine turnover rates. The mechanism revealed by our study would serve a molecular basis to explain those events concerning spine remodeling through a perspective of F-actin dynamics.

CORT downregulated the CaD expression levels in hippocampal neurons and suppressed the fibro-type CaD promoter's SRF/CArG-box-dependent activity (Fig. 6). In this regard, activated GR inhibits SRF activity in human prostate adenocarcinoma cells (Yemelyanov et al., 2007). We previously demonstrated that GC upregulates CaD expression via positive GRE-like sequences in both human lung cancer cells and cortical neural progenitor cells (Mayanagi et al., 2008; Fukumoto et al., 2009). However, in hippocampal neurons the GRE-like sequences did not function for the negative regulation of CaD transcription and the direct contribution of GR via the GRE-like sequences, therefore, seems to be less significant. These different responses against GC may be due to cellular contexts. This mechanism is required for future analysis.

As documented here, CaD plays an important role in synaptic plasticity as well, because CaD is required for synaptic remodeling accompanied with chemically induced LTP. CaD plays also a role as a crucial downstream target in the stress/GC-induced effects on dendritic spine development. The abnormality of spine structure is considered to be associated with pathological dysfunction of the synapse. Indeed, psychiatric and neurologic disorders such as depression, schizophrenia, and Alzheimer's disease are characterized by pathologically altered spines (van Spronsen and Hoogenraad, 2010; Penzes et al., 2011). Thus, CaD may be involved in the stress-induced psychiatric disorders. Since spines and dendrites in young or aged rat brains are reported to exhibit different responsiveness against chronic stress (Dumitriu et al., 2010; Bloss et al., 2011), future study is required for this mechanism involving CaD. Our present study provides new insight into the molecular basis of stress/GC-induced synaptic remodeling, and detailed investigation of the relationship between stress/GCs and CaD should improve our understanding of stress-induced neuronal plasticity and the related psychiatric disorders.

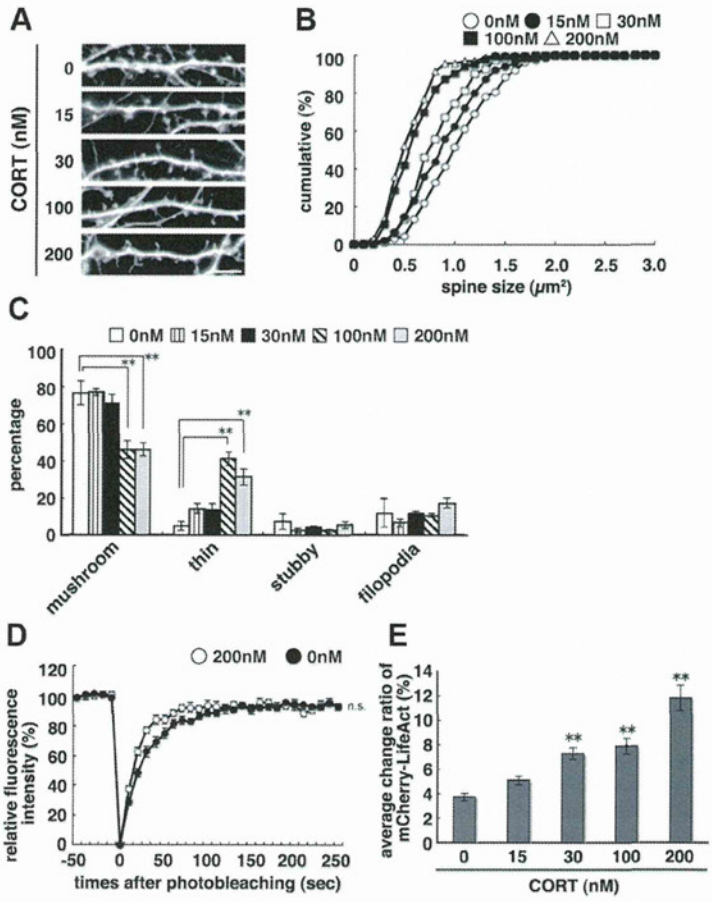

Figure 7. CORT effects on spine morphology and dynamics. ***A***, Spine morphology in GFP-transfected hippocampal neurons cultured with 0–200 nM CORT (scale bar, 10 μm); (***B***) the graph shows spine sizes and their cumulative distributions. ***C***, Dendritic protrusions, categorized by morphology: mushroom, thin, stubby, and filopodial. Data are means ± SE of values from at least 183 spines. ***D***, The fluorescence recovery of mCherry-β-actin over time after photobleaching, measured in neurons cultured with 0 or 200 nM CORT. Data are means ± SE of values from 12 cells. ***E***, CORT dose-dependent effects on spine F-actin dynamics were measured using mCherry-LifeAct. The graph shows the change rates of mCherry-LifeAct fluorescence intensity in spines. Data are means ± SE of values from at least 27 spines (**$p < 0.01$).

References

Becker JB, Monteggia LM, Perrot-Sinal TS, Romeo RD, Taylor JR, Yehuda R, Bale TL (2007) Stress and disease: is being female a predisposing factor? J Neurosci 27:11851–11855.

Bloss EB, Janssen WG, Ohm DT, Yuk FJ, Wadsworth S, Saardi KM, McEwen BS, Morrison JH (2011) Evidence for reduced experience-dependent dendritic spine plasticity in the aging prefrontal cortex. J Neurosci 31: 7831–7839.

Dumitriu D, Hao J, Hara Y, Kaufmann J, Janssen WG, Lou W, Rapp PR, Morrison JH (2010) Selective changes in thin density and morphology in monkey prefrontal cortex correlate with aging-related cognitive impairment. J Neurosci 30:7507–7515.

Fischer M, Kaech S, Knutti D, Matus A (1998) Rapid actin-based plasticity in Dendritic spines. Neuron 20;847–854.

Fischer M, Kaech S, Wagner U, Brinkhaus H, Matus A (2000) Glutamate receptors regulate actin-based plasticity in dendritic spines. Nat Neurosci 3: 887–894.

Fukumoto K, Morita T, Mayanagi T, Tanokashira D, Yoshida T, Sakai A, Sobue K (2009) Detrimental effects of glucocorticoids on neuronal migration during brain development. Mol Psychiatry 14:1119–1131.

Gu J, Lee CW, Fan Y, Komlos D, Tang X, Sun C, Yu K, Hartzell HC, Chen G, Bamburg JR, Zheng JQ (2010) ADF/cofilin-mediated actin dynamics regulate AMPA receptor trafficking during synaptic plasticity. Nat Neurosci 13:1208–1215.

Hotulainen P, Hoogenraad CC (2010) Actin in dendritic spines: connecting dynamics to function. J Cell Biol 189:619–629.

Jiang M, Chen G (2006) High Ca^{2+}-phosphate transfection efficiency in low-density neuronal cultures. Nat Protoc 1:695–700.

Korkotian E, Segal M (2001) Regulation of dendritic spine motility in cultured hippocampal neurons. J Neurosci 21:6115–6124.

Lisman J (2003) Actin's actions in LTP-induced synapse growth. Neuron 38:361–362.

Liston C, Gan WB (2011) Glucocorticoids are critical regulators of dendritic spine development and plasticity in vivo. Proc Natl Acad Sci U S A 108: 16074–16079.

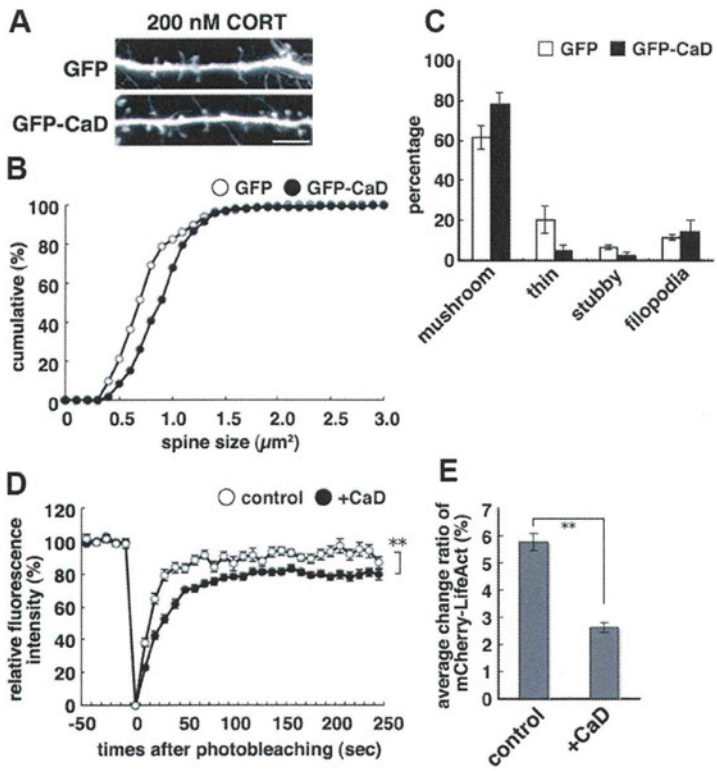

Figure 8. CaD recovers the CORT-induced dendritic spine changes. ***A***, Spine morphology in neurons cultured with 200 nM CORT and transfected with GFP or GFP-CaD (scale bar, 10 μm); (***B***) the graph shows spine sizes and their cumulative distributions. ***C***, Dendritic protrusions, classified by morphology: mushroom, thin, stubby, and filopodial. Data are means ± SE of values from at least 1214 spines. ***D***, The fluorescence recovery of mCherry-β-actin over time after photobleaching, measured in neurons cultured with 200 nM CORT and transfected with a mock vector (control) or myc-tagged-CaD. Data are means ± SE of values from 16 cells (**$p < 0.01$). ***E***, Spine F-actin dynamics in neurons cultured with 200 nM CORT and transfected by mock vector (control) or myc-tagged-CaD were measured using mCherry-LifeAct. The graph shows the change rates of mCherry-LifeAct fluorescence intensity in spines. Data are means ± SE of values from at least 21 spines (**$p < 0.01$).

Magariños AM, McEwen BS, Flügge G, Fuchs E (1996) Chronic psychosocial stress causes apical dendritic atrophy of hippocampal CA3 pyramidal neurons in subordinate tree shrews. J Neurosci 16:3534–3540.

Mayanagi T, Sobue K (2011) Diversification of caldesmon-linked actin cytoskeleton in cell motility. Cell Adh Migr 5:150–159.

Mayanagi T, Morita T, Hayashi K, Fukumoto K, Sobue K (2008) Glucocorticoid receptor-mediated expression of caldesmon regulates cell migration via the reorganization of the actin cytoskeleton. J Biol Chem 283:31183–31196.

McEwen BS (1999) Stress and hippocampal plasticity. Annu Rev Neurosci 22:105–122.

McEwen BS (2005) Glucocorticoids, depression, and mood disorders: structural remodeling in the brain. Metabolism 54:20–23.

McEwen BS (2010) Stress, sex, and neural adaptation to a changing environment: mechanisms of neuronal remodeling. Ann N Y Acad Sci 1204:E38–E59.

Modi N, Lewis H, Al-Naqeeb N, Ajayi-Obe M, Doré CJ, Rutherford M (2001) The effects of repeated antenatal glucocorticoid therapy on the developing brain. Pediatr Res 50:581–585.

Morita T, Mayanagi T, Sobue K (2012) Caldesmon regulates axon extension through interaction with Myosin II. J Biol Chem 287:3349–3356.

Otmakhov N, Khibnik L, Otmakhova N, Carpenter S, Riahi S, Asrican B, Lisman J (2004) Forskolin-induced LTP in the CA1 hippocampal region is NMDA receptor dependent. J Neurophysiol 91:1955–1962.

Penzes P, Cahill ME, Jones KA, VanLeeuwen JE, Woolfrey KM (2011) Dendritic spine pathology in neuropsychiatric disorders. Nat Neurosci 14:285–293.

Phillips NK, Hammen CL, Brennan PA, Najman JM, Bor W (2005) Early adversity and the prospective prediction of depressive and anxiety disorders in adolescents. J Abnorm Child Psychol 33:13–24.

Radley JJ, Sisti HM, Hao J, Rocher AB, McCall T, Hof PR, McEwen BS, Morrison JH (2004) Chronic behavioral stress induces apical dendritic reorganization in pyramidal neurons of the medial prefrontal cortex. Neuroscience 125:1–6.

Radley JJ, Rocher AB, Miller M, Janssen WG, Liston C, Hof PR, McEwen BS, Morrison JH (2006) Repeated stress induces dendritic spine loss in the rat medial prefrontal cortex. Cereb Cortex 16:313–320.

Sarmiere PD, Bamburg JR (2004) Regulation of the neuronal actin cytoskeleton by ADF/cofilin. J Neurobiol 58:103–117.

Sobue K, Sellers JR (1991) Caldesmon, a novel regulatory protein in smooth muscle and nonmuscle actomyosin systems. J Biol Chem 266:12115–12118.

Star EN, Kwiatkowski DJ, Murthy VN (2002) Rapid turnover of actin in dendritic spines and its regulation by activity. Nat Neurosci 5:239–246.

van Spronsen M, Hoogenraad CC (2010) Synapse pathology in psychiatric and neurologic disease. Curr Neurol Neurosci Rep 10:207–214.

von Bohlen Und Halbach O (2009) Structure and function of dendritic spines within the hippocampus. Ann Anat 191:518–531.

Watanabe Y, Gould E, McEwen BS (1992) Stress induces atrophy of apical dendrites of hippocampal CA3 pyramidal neurons. Brain Res 588:341–345.

Weinstock M (2008) The long-term behavioural consequences of prenatal stress. Neurosci Biobehav Rev 32:1073–1086.

Wellman CL (2001) Dendritic reorganization in pyramidal neurons in medial prefrontal cortex after chronic corticosterone administration. J Neurobiol 49:245–253.

Yano H, Hayashi K, Haruna M, Sobue K (1994) Identification of two distinct promoters in the chicken caldesmon gene. Biochem Biophys Res Commun 201:618–626.

Yemelyanov A, Czwornog J, Chebotaev D, Karseladze A, Kulevitch E, Yang X, Budunova I (2007) Tumor suppressor activity of glucocorticoid receptor in the prostate. Oncogene 26:1885–1896.

THE JOURNAL OF BIOLOGICAL CHEMISTRY VOL. 287, NO. 5, pp. 3349–3356, January 27, 2012

Caldesmon Regulates Axon Extension through Interaction with Myosin II*

Received for publication, August 18, 2011, and in revised form, November 27, 2011 Published, JBC Papers in Press, December 9, 2011, DOI 10.1074/jbc.M111.295618

Tsuyoshi Morita[‡], **Taira Mayanagi**[‡§], **and Kenji Sobue**[‡§1]

From the [‡]*Department of Neuroscience, Osaka University Graduate School of Medicine, 2-2 Yamadaoka, Suita, Osaka 565-0871, Japan and the* [§]*Department of Neuroscience, Institute for Biomedical Sciences, Iwate Medical University, 2-1-1 Nishitokuta, Yahaba-cho, Shiwa-gun, Iwate 028-3694, Japan*

Background: Axon extension, an essential step for creating neural circuits, is regulated by cytoskeletal dynamics.
Results: Caldesmon is a regulator of the actin cytoskeleton and enhances axon extension through direct interaction with myosin II.
Conclusion: Caldesmon binding to myosin II inhibits myosin II function, resulting in the enhancement of axon extension.
Significance: This study elucidates how caldesmon-regulated actin-myosin system is involved in axon extension.

To begin the process of forming neural circuits, new neurons first establish their polarity and extend their axon. Axon extension is guided and regulated by highly coordinated cytoskeletal dynamics. Here we demonstrate that in hippocampal neurons, the actin-binding protein caldesmon accumulates in distal axons, and its N-terminal interaction with myosin II enhances axon extension. In cortical neural progenitor cells, caldesmon knockdown suppresses axon extension and neuronal polarity. These results indicate that caldesmon is an important regulator of axon development.

Neurons in the developing brain extend axonal and dendritic arbors that create a complex circuitry, and the guided extension of axonal fibers is an essential step in this process. Axon extension is regulated by the coordinated interaction of microtubules and actin filaments in the axonal growth cone. A growing body of evidence indicates that microtubule polymerization and stabilization play positive roles in axon extension (1), whereas actin filament roles are more complicated. For example, knocking out Ena/VASP or Cdc42, which positively regulate actin polymerization, causes axonal tract loss (2, 3). In contrast, inhibiting the actin nucleation factor Arp2/3 and pharmacologically destabilizing actin filaments enhances axon extension (4, 5). Thus, the fundamental details of axon guidance and regulation by actin filaments are not well understood.

Caldesmon (CaD)[2] was first identified as a smooth-muscle protein that binds calmodulin and actin (6). It has since been found to be ubiquitously expressed in smooth muscle and nonmuscle cells, and to regulate Ca^{2+}-dependent actomyosin contraction (7, 8). CaD binds to the side of filamentous actin (F-actin) and inhibits actin-myosin interactions, as revealed by superprecipitation assays and actin-activated myosin ATPase activity (9–11). CaD binding also stabilizes F-actin filaments by enhancing actin-tropomyosin binding and preventing the actin-severing activity of gelsolin or cofilin (12, 13). CaD plays important roles in migration of non-muscle cells via regulating actin-myosin system (8). We recently reported that CaD is involved in detrimental glucocorticoid-induced effects during cortical brain development (14, 15): glucocorticoids increase CaD levels, transiently retarding the radial migration of cortical neuronal progenitor cells. We also reported that CaD localizes to neuronal growth cones (16). Thus, it seems that CaD plays multiple important roles in neuronal development. In this report, we demonstrate a novel role for CaD in axon extension via its N-terminal myosin binding sequence.

EXPERIMENTAL PROCEDURES

Materials—The myosin II ATPase inhibitor blebbistatin, the myosin light chain kinase inhibitor ML-7, and the Rho-associated protein kinase inhibitor Y27632 were purchased from Merck. The following antibodies were purchased: anti-tau1 (Chemicon), anti-MAP2 (Chemicon), anti-nonmuscle myosin IIA (Abcam), anti-nonmuscle myosin IIB (Abcam), anti-GFP (Invitrogen), anti-FLAG (Sigma), anti-Myc (9E10, Santa Cruz Biotechnology), and anti-GAPDH (FL-335, Santa Cruz Biotechnology). Anti-CaD antibody was generated as previously described (17).

Cell Culture and Immunostaining—Hippocampal neurons were prepared from rat hippocampi on embryonic day 18.5. The dissociated neurons were plated on poly-L-lysine-coated coverslips, and cultured in glial-conditioned MEM containing 1 mM pyruvate, 0.6% (w/v) D-glucose, and 2% B27 supplement (Invitrogen). The next day, the culture was changed to a neurobasal medium containing 2% B27 supplement and 0.5 mM L-glutamine. Cortical NPCs were prepared from rat cerebral cortex on embryonic day 15.5 (E15.5), cultured as previously described (14), plated on laminin-coated coverslips, and cultured under basic FGF-free conditions to induce their differentiation into polarized neurons. A549 and HEK293T cells were cultured in Dulbecco's modified Eagle's medium supplemented with 10% fetal calf serum. Cells cultured on coverslips were fixed using 4% paraformaldehyde and then processed for immunocyto-

* This work was supported by Grants-in-aid for Scientific Research 20240038 from the Japan Society for the Promotion of Science (to K. S.) and 23110510 from the Ministry of Education, Culture, Sports, Science and Technology (MEXT) (to K. S.).

[1] To whom correspondence should be addressed: Dept. of Neuroscience, Institute for Biomedical Sciences, Iwate Medical University, 2-1-1 Nishitokuta, Yahaba-cho, Shiwa-gun, Iwate 028-3694, Japan. Tel.: 81-19-651-5710; Fax: 81-19-908-8020; E-mail: ksobue@iwate-med.ac.jp.

[2] The abbreviations used are: CaD, caldesmon; DIV, day *in vitro*; NPCs, neural progenitor cells; FGF, fibroblast growth factor; HMM, heavy meromyosin.

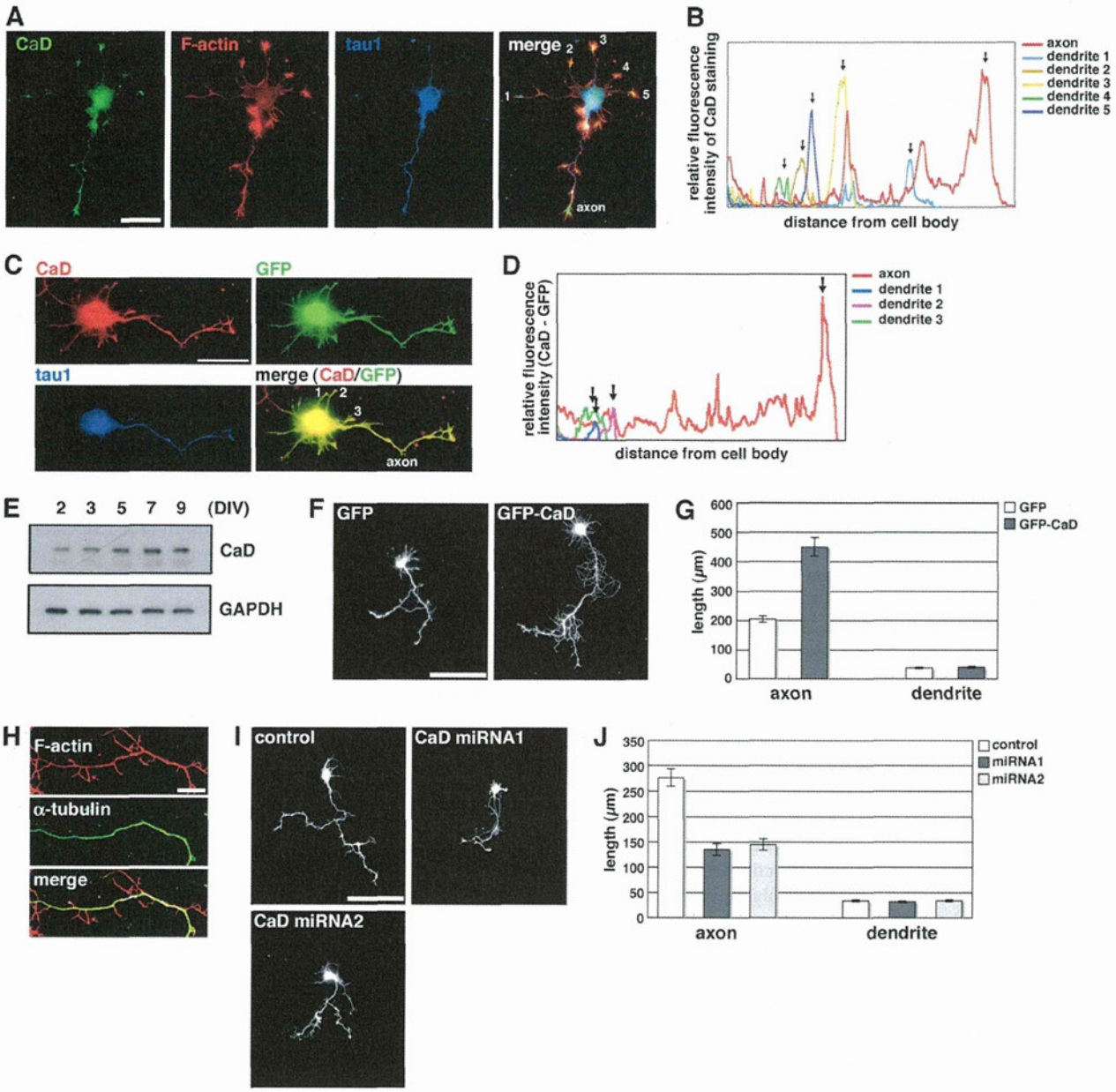

FIGURE 1. **CaD involvement in axon extension.** *A*, CaD protein localization in primary cultured hippocampal neurons. The neurons were fixed and triple-stained with anti-CaD, anti-tau1 antibodies, and phalloidin (F-actin). Bar, 50 μm. *B*, dendrite and axon fluorescence intensities measured in the CaD-immunostained image shown in *A*; *arrows* indicate growth cones. *C*, neurons, which had been transfected with GFP as a cell volume maker, were fixed and triple-stained with anti-CaD, anti-GFP, and anti-tau1 antibodies. Bar, 50 μm. *D*, dendrite and axon fluorescence intensities were measured in the CaD-immunostained and GFP-immunostained images shown in *C*, respectively, and then GFP-intensity was subtracted from CaD-intensity to correct for the influence of cell volume. *Arrows* indicate growth cones. *E*, changes in CaD protein expression during neuronal development. *F*, morphology of GFP- or GFP-CaD-transfected neurons after 3 days in culture (bar, 100 μm) and *G*, quantification of their axonal and dendritic length. Axonal length represents the longest axon branch. Data are means ± S.E. from six independent experiments. *H*, morophlogy of CaD-induced filopodia-like protrusions. The myc-CaD-transfected neurons were fixed and stained with anti-tubulin and phalloidin (F-actin). Bar, 25 μm. *I*, morphology of neurons transfected with control miRNA, CaD miRNA1, or CaD miRNA2, and cultured for 5 days (bar, 100 μm), and *J*, quantification their axonal and dendritic lengths. Data are means ± S.E. from four to six independent experiments.

chemistry. To label F-actin, Alexa 568-phalloidin (Molecular Probes) was added to the secondary antibody solution.

Transfection—Hippocampal neurons prepared from rat embryos on E18.5 were transfected by the calcium phosphate method as described previously (18). In brief, DNA-calcium phosphate precipitates were prepared using a calcium phosphate transfection kit (Invitrogen). The hippocampal neurons were plated on a Nunclon Δ surface plate (Nalge Nunc International) and incubated with the precipitates for 3 h. The transfected neurons were replated on poly-L-lysine-coated coverslips and cultured for 3 to 5 days. A549 and HEK293T cells were transfected using Lipofectamine 2000 or Lipofectamine LTX (Invitrogen).

Expression Plasmids—The coding regions for human l-CaD, its N terminus (1–263 amino acids), C terminus (264–558 amino acids), and N terminus Δ21–47 (lacking amino acids

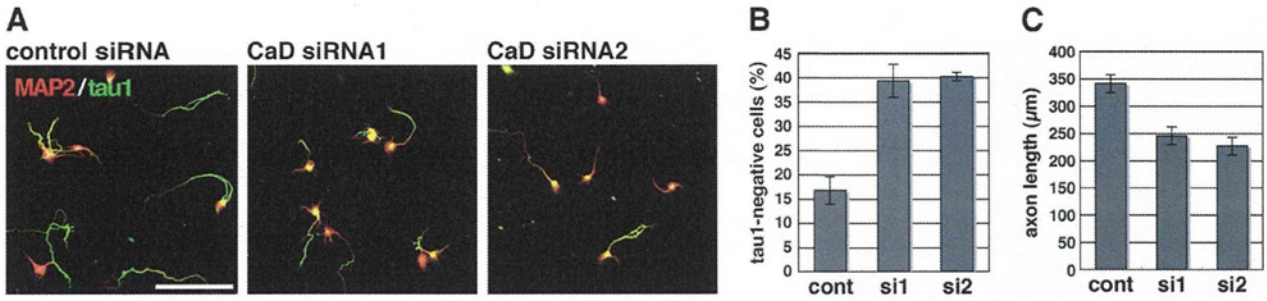

FIGURE 2. **CaD involvement in cortical NPC axon development.** *A*, proliferating cortical NPCs were incubated with control siRNA, CaD siRNA1, or CaD siRNA2 for 3 days, and cultured in basic FGF-free medium for 3 days. The cultured cells were fixed and stained with anti-tau1 (*green*) and anti-MAP2 (*red*) antibodies. Bar, 200 μm. *B*, percentage of tau1-negative non-polarized cells among the differentiating progenitor cells. Data are means ± S.E. from at least 120 cells. *C*, quantification of axonal length in tau1-positive cells. Data are means ± S.E. from at least 30 cells.

21–47 from the N terminus), and the N-terminal fragments of rat myosin IIA (1–1961 amino acids) and IIB (1–1976 amino acids) were amplified by PCR and subcloned into the highly efficient mammalian expression plasmid pCAGGS. EGFP and Myc tag sequences were fused to the 5′-end of the coding sequences. The mcherry-LifeAct expression vector was constructed as previously reported (19).

RNA Interference—Short-interfering RNAs (siRNAs) against rat CaD were transfected into growing cortical NPCs using Lipofectamine RNAi MAX (Invitrogen). MicroRNA (miRNA) plasmids against rat CaD were constructed as previously described (14) and transfected into hippocampal neurons by calcium phosphate precipitation. The targeting sequences and the siRNA and miRNA knockdown efficacy were reported in our previous studies (14, 20).

Immunoprecipitation—HEK293T cells with transfected expression vectors were lysed with Triton-X-buffer (0.05% Triton X-100 (pH 7.6), 30 mM Tris-HCl, 50 mM NaCl 5 mM EGTA, 5 mM $MgCl_2$, 1 mM ATP, and protease inhibitor mixture for use with mammalian cell and tissue extracts (Nacalai Tesque)). Immunoprecipitation was performed using the earlier-listed antibodies and protein G-Sepharose (GE Healthcare Life Sciences). The Sepharose beads were boiled in SDS-sample buffer to elute the immunocomplexes.

RESULTS

CaD Enhances Axon Extension in Hippocampal Neurons—CaD, a ubiquitous regulator of the actin cytoskeleton, localizes along actin fibers and in the ruffling membrane (7, 8). Here, we found that CaD was located in the soma and growth cones of primary cultured hippocampal neurons, with the strongest expression in the distal axon (Fig. 1, *A–D*). CaD levels increased for 3 to 7 days *in vitro* (DIV) (2.3 ± 0.8-fold at 7 DIV *versus* 2 DIV) while the neurons established polarity and actively extended axons (Fig. 1*E*). The location and time-course of CaD expression in these cells are consistent with its having a role in axon extension.

We therefore investigated CaD function in neurite outgrowth by overexpressing or knocking down CaD in hippocampal neurons. We used GFP-fused CaD (GFP-CaD), which has the same functions as endogenous CaD (14, 20). GFP-CaD dramatically enhanced axon extension but did not significantly affect dendrite length as compared with the control, GFP (Fig. 1, *F* and *G*). GFP-CaD also enhanced formation of filopodia-like protrusions from the soma and axon branches (Fig. 1*F*). These CaD-induced protrusions were composed of concentrated actin filaments and were distinct from the main axonal branches, which were filled with microtubules (Fig. 1*H*). Knocking down the endogenous CaD decreased axon length, but not dendritic length (Fig. 1, *I* and *J*), indicating that CaD accumulates in the distal axon of hippocampal neurons during their development and enhances axon extension.

CaD Regulates Axon Development in Cortical NPCs—To monitor CaD involvement in early events in neurite outgrowth, we used cortical neural progenitor cells (NPCs), which proliferate as non-polarized cells in the presence of basic fibroblast growth factor (FGF) (14, 21). Under basic FGF-free conditions, however, NPCs stop proliferating and establish neuronal polarity with MAP2-positive dendrites and a tau1-positive axon (Fig. 2*A*). When CaD was knocked down with siRNAs in proliferating NPCs, tau1-staining showed that the establishment of neuronal polarity was significantly suppressed within three culture days under basic FGF-free conditions (Fig. 2, *A* and *B*). Even in polarized cells, the length of tau1-positive axons was significantly shortened by CaD knockdown (Fig. 2, *A* and *C*), as observed in hippocampal neurons. At an early stage of NPCs differentiation into polarized cells, immature axons were often stained with both anti-MAP2 and anti-tau1 antibodies. In the CaD-knockdown NPCs, some short axons were MAP2/tau1 double positive, suggesting delayed development of these cells. These findings indicate that CaD plays important roles in establishing neuronal polarity and in axon extension in developing NPCs.

CaD-Myosin Interaction Required for Axon Extension—CaD has been reported to bind smooth muscle myosin at its N terminus and F-actin at its C terminus, suggesting that it functions to link these molecules (22). In the growth cone of hippocampal neuronal axons, CaD colocalized with F-actin and myosin IIA/IIB, the major non-muscle isoforms of myosin II (Fig. 3*A*). To examine myosin and actin involvement in CaD-induced axon extension, CaD N- and C-terminal fragments (N-CaD and C-CaD) were expressed separately in hippocampal neurons. N-CaD enhanced axon extension like full-length CaD, but C-CaD did not (Fig. 3, *B–D*), suggesting that CaD interaction with myosin, but not F-actin, is necessary for CaD-induced axon extension. On the other hand, C-CaD, but not N-CaD, induced formation of the filopodia-like protrusions like full-

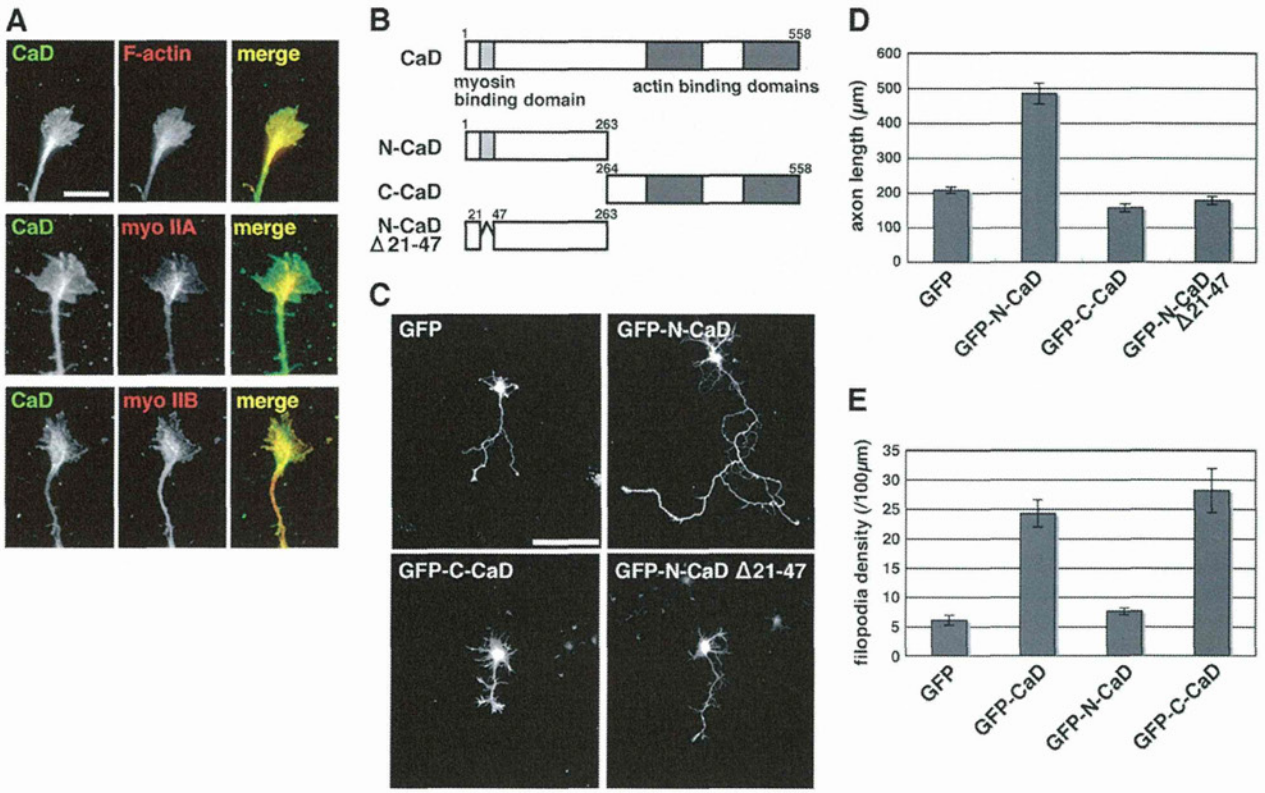

FIGURE 3. **The effect of CaD N- and C-terminal fragments on axon extension.** *A*, CaD, myosin IIA, and myosin IIB localization in the hippocampal neuron axonal growth cone. Bar, 10 μm. *B*, CaD domain structure. *C*, morphology of neurons cultured for 3 days after transfection with GFP, GFP-N-CaD, GFP-C-CaD, or GFP-N-CaD Δ21–47 (bar, 100 μm.), and *D*, quantification of their axonal length. Data are means ± S.E. of values from four to six independent experiments. *E*, quantification of their filipodial density. Data are means ± S.E. of values from four to six independent experiments.

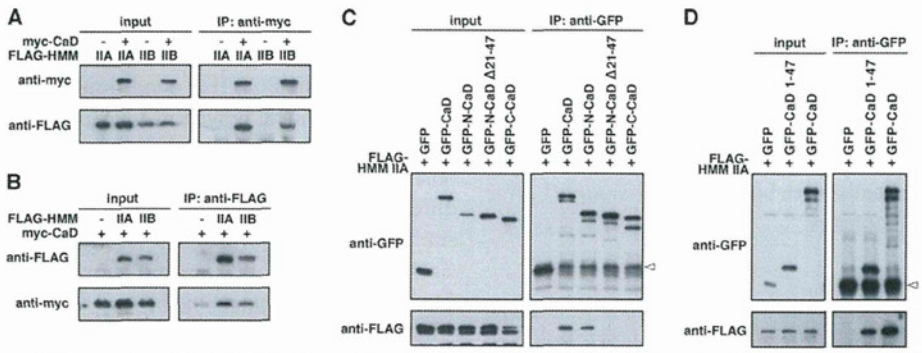

FIGURE 4. **CaD and myosin II interactions.** *A*, HEK 293T cells transfected with myc-CaD and FLAG-HMM IIA or FLAG-HMM IIB were immunoprecipitated using anti-Myc antibody or *B*, anti-FLAG antibody. *C*, HEK 293T cells were transfected with FLAG-HMM IIA and GFP, GFP-CaD, GFP-N-CaD, GFP-N-CaD Δ21–47, or GFP-C-CaD and immunoprecipitated with anti-GFP antibody. *Arrowhead*: IgG light chain position. *D*, HEK 293T cells were transfected with FLAG-HMM IIA and GFP, GFP-CaD Δ21–47, or GFP-CaD and immunoprecipitated with anti-GFP antibody. *Arrowhead*: IgG light chain position.

length CaD (Figs. 1*F* and 3, *C* and *E*), suggesting that this effect is dependent on the C-terminal actin binding domains.

Co-immunoprecipitation was used to determine whether non-muscle myosin II, like smooth- and skeletal-muscle myosins, binds to CaD. Because CaD is reported to bind to the S-1 and S-2 regions of smooth and skeletal muscle myosins (23), we examined CaD interactions with myosin IIA or IIB N-terminal fragments, which are composed of a globular head domain, a neck region, and a small tail fragment corresponding to heavy meromyosin (HMM). As with smooth and skeletal muscle myosins, CaD bound to HMM IIA and IIB, and CaD's C-terminal F-actin-binding domains were not necessary for these interactions (Fig. 4, *A–C*).

Previous studies demonstrated that the 27-amino acid sequence in CaD's N terminus (Tyr-21 to Lys-47 in human l-CaD) is necessary for binding to smooth-muscle myosin (24). N-CaD Δ21–47 fragment, in which this 27-amino acid sequence is deleted, did not interact with HMM IIA, and a CaD fragment including amino acids 1–47 was the minimum required for HMM IIA binding (Fig. 4, *C* and *D*). Importantly, N-CaD Δ21–47 fragment completely lost the ability to enhance axon extension (Fig. 3, *C* and *D*), strongly supporting the idea that CaD is accumulated in the growth cone as

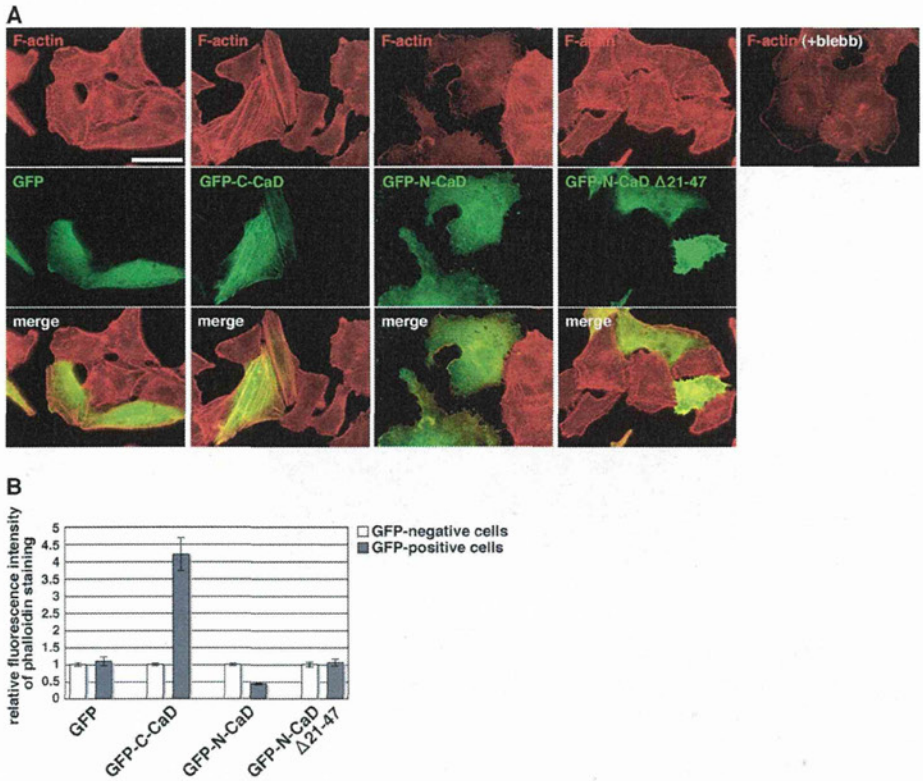

FIGURE 5. **CaD fragments ectopically expressed in A549 cells.** A549 cells transfected with GFP, GFP-C-CaD, GFP-N-CaD, or GFP-N-CaD Δ21–47 were fixed and stained with anti-GFP antibody (*green*) and phalloidin (F-actin, *red*). At right, cells were treated with 10 μM blebbistatin (blebb) for 30 min and then fixed and stained with phalloidin. Bar, 100 μm. *B*, quantification of fluorescence intensity of phalloidin staining in GFP-positive and GFP-negative cells, respectively.

an actomyosin component and enhances axon extension through direct interaction with non-muscle myosin II.

N-CaD Exhibits the Same Effect as Blebbistatin—To determine the significance of CaD interaction with myosin, N-CaD or C-CaD was transfected into A549 cells. CaD has been reported to stabilize actin filaments via its C-terminal F-actin-binding domains, causing thick actin fibers to form (12, 26). In A549 cells, C-CaD strongly induced thick actin fiber formation (Fig. 5, *A* and *B*). On the other hand, cells expressing N-CaD showed significant actin fiber loss and a flat cell shape with prominent lamellipodia (Fig. 5, *A* and *B*). These effects were completely lost in A549 cells expressing an N-CaD Δ21–47 fragment lacking the 27-amino acid myosin-binding sequence (Fig. 5, *A* and *B*). Further, these morphological changes were very similar to those found in cells treated with the myosin II-inhibitor blebbistatin (Fig. 5*A*). These results suggest that CaD binds to myosin at its N terminus, and that it inhibits myosin II function independently of its C-terminal F-actin-binding domains.

CaD Changes Growth Cone Morphology and Myosin II Localization—To determine the function of CaD in growth cones, we observed growth cone morphology and myosin II localization in the hippocampal neurons expressing CaD fragments (Fig. 6). N-CaD inhibited lamellipodia expansion, whereas C-CaD enhanced filopodia formation in growth cones. Full-length CaD induced both lamellipodia retraction and filopodia formation. N-CaD Δ21–47 had no effect on growth cone morphology.

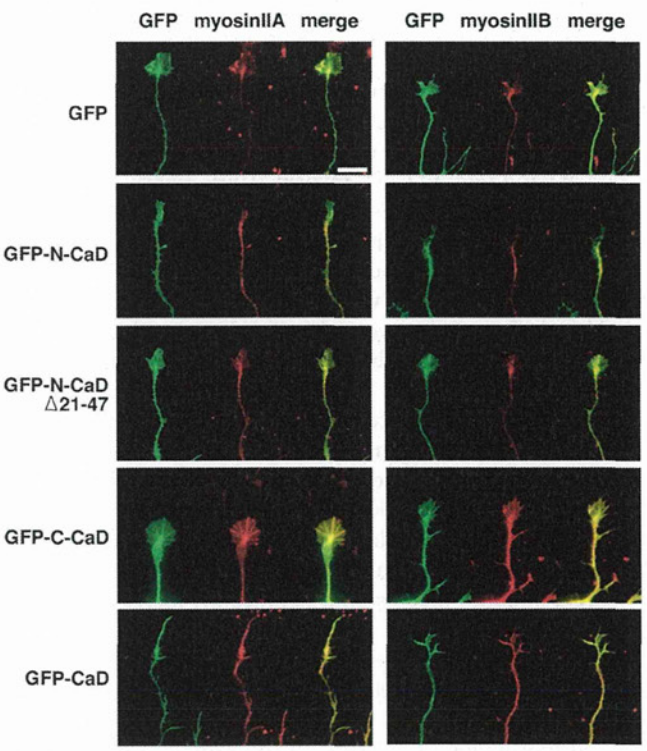

FIGURE 6. **The effect of CaD fragments on growth cone morphology and myosin II localization.** Hippocampal neurons transfected with GFP, GFP-C-CaD, GFP-N-CaD, GFP-N-CaD Δ21–47, or GFP-CaD were fixed and stained with anti-GFP (*green*) and anti-myosin IIA or IIB (*red*) antibodies. Bar, 10 μm.

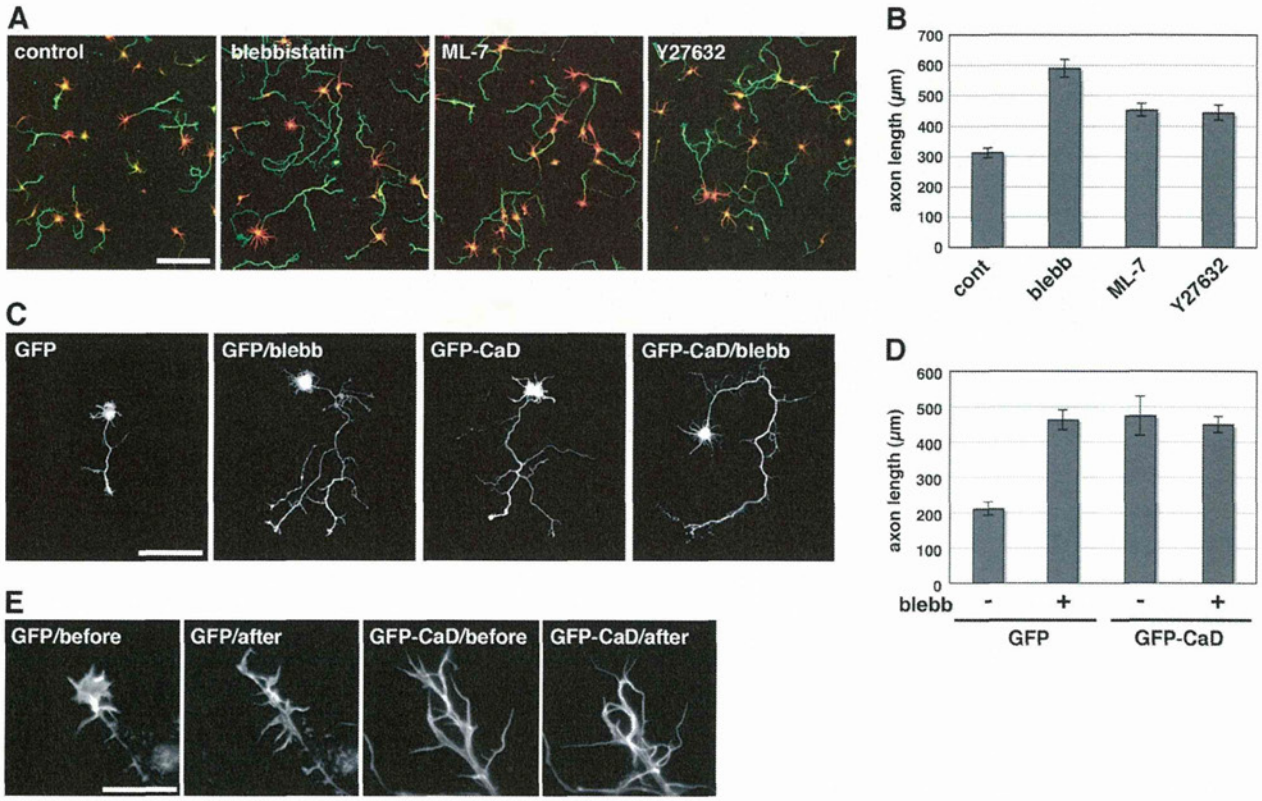

FIGURE 7. **Myosin II functions in CaD-enhanced axon extension.** *A*, hippocampal neurons were cultured with 10 μM blebbistatin, 50 μM ML-7, or 10 μM Y27632 for 3 days, and then fixed and stained with anti-tau1 (*green*) and anti-MAP2 (*red*) antibodies (bar, 400 μm.); *B*, quantification of axonal length in these neurons. Data are means ± S.E. of values from at least 70 cells. *C*, primary cultured hippocampal neurons transfected with GFP or GFP-CaD and incubated with or without 10 μM blebbistatin for 3 days (bar, 100 μm); *D*, quantification of axonal length in these neurons. Data are means ± S.E. from four independent experiments. *E*, growth cone morphology in GFP- or GFP-CaD-transfected neurons before or after treatment with 10 μM blebbistatin for 30 min. To visualize F-actin in living neurons, the cells were transfected with mcherry-LifeAct. Bar, 20 μm.

In GFP-N-CaD-transfected neurons, myosin II staining was slightly diffuse, but distinctly strong in the basal region of the lamellipodia-poor growth cones. In the cells transfected with GFP-CaD and GFP-C-CaD, myosin II was tightly associated with filopodia. N-CaD Δ21–47 had no effect on myosin II localization. These results indicate that C-terminal actin binding domains enhances actin bundling in growth cones, leading to filopodia formation, with which myosin II associates. On the other hand, N-terminal myosin-binding domain inhibits lamellipodia formation in growth cone, but scarcely have an effect on the myosin II localization.

CaD Enhances Axon Extension by Inhibiting Myosin—To examine how inhibiting myosin function would affect axon extension, hippocampal neurons were incubated with blebbistatin, myosin light chain kinase inhibitor ML-7, or Rho-associated protein kinase inhibitor Y27632, drugs that directly or indirectly inhibit myosin function. All of these drugs, especially the direct inhibitor blebbistatin, significantly increased axonal length compared with the vehicle control (Fig. 7, *A* and *B*). In GFP-CaD-transfected hippocampal neurons, however, blebbistatin did not further accelerate axon extension (Fig. 7, *C* and *D*). Coupled with its effects on axon extension, blebbistatin induced morphological changes in the axonal growth cones, inducing a switch from lamellipodial to filopodia-like protrusions (Fig. 7*E*). In the GFP-CaD-transfected neurons, axonal growth cones displayed a filopodia-like morphology without expanded lamellipodia, and their morphology was not affected by blebbistatin treatment (Fig. 7*E*). These findings indicate that blebbistatin and CaD enhance axon extension via the same pathway, through which myosin II function is inhibited.

DISCUSSION

CaD is a ubiquitous regulator of the actin cytoskeleton. Most of CaD functional domains that bind F-actin, tropomyosin, and calmodulin are located in its C terminus, and the C-terminal fragment can inhibit myosin ATPase activity and stabilize actin filaments (8, 12, 26–28). CaD N-terminal region also has a myosin-binding sequence, through which CaD binds to smooth and skeletal muscle heavy meromyosins (23). This binding domain is probably involved in tethering myosin to actin filaments (22, 29), but the significance of myosin binding to CaD had been unclear. In our present study, we clearly demonstrated that CaD enhances axon extension through direct interaction with non-muscle myosin II via its N-terminal myosin-binding sequence. N-CaD, which lacks the all C-terminal functional domains, exhibited the same effect on axon extension as full-length CaD (Fig. 3, *C* and *D*), indicating that axon extension does not depend on the CaD-mediated physical bridge between myosin and actin.

In addition to axon extension, CaD induced formation of the filopodia-like protrusions from soma and axon branches (Figs. 1*F* and 3*E*). CaD also enhanced filopodia formation in growth

cones (Fig. 6). C terminus of CaD, but not N terminus, was required for both functions. C terminus contains some actin binding domains, which are necessary for stabilization of actin bundles (7, 8), and the filopodia-like protrusion were composed of concentrated actin filaments (Fig. 1*H*). These indicate that actin stabilization by the C-terminal domains facilitates formation of these filopodial protrusions independently of N-terminal myosin binding domain.

Results of our experiments using myosin II ATPase inhibitor blebbistatin strongly suggest an inhibitory effect of N-CaD on myosin II function in hippocampal neurons and non-neuronal A549 cells (Figs. 5 and 7). However, previous *in vitro* study showed that the CaD^{1-597} fragment, which lacks the C-terminal actin-binding domains, does not inhibit actin-activated myosin ATPase activity (29). Velaz *et al.* (22) reported that CaD inhibits actin-activated myosin ATPase activity via its C-terminal F-actin-binding domains, by preventing the myosin head from binding to actin *in vitro* (21). Considering the discrepancy between these *in vitro* studies and our *in vivo* study, we propose that N-CaD inhibits myosin II function by unknown mechanisms, which may include interacting with or recruiting additional myosin-inhibitory factors. Further investigations are required to clarify how N-CaD inhibits myosin II function.

Growing evidences indicate that myosin II function is important for axon outgrowth and axon guidance (30–35). However, the molecular mechanism underlying actomyosin-mediated axon extension has not been fully evaluated. An early study by Letourneau *et al.* (36) clearly demonstrated that both "push" by microtubules and "pull" by actomyosin in the growth cone play central roles in axon extension. Actually, actin destabilization by cytochalasin D or ADF/cofilin and myosin II inhibition by blebbistatin enhance axon extension (Refs. 5, 25 and the present study). CaD may inhibit the traction force generated by the actomyosin contraction, thereby augmenting the pushing force from microtubule extension.

REFERENCES

1. Poulain, F. E., and Sobel, A. (2010) The microtubule network and neuronal morphogenesis: Dynamic and coordinated orchestration through multiple players. *Mol. Cell. Neurosci.* **43,** 15–32
2. Kwiatkowski, A. V., Rubinson, D. A., Dent, E. W., Edward van Veen, J., Leslie, J. D., Zhang, J., Mebane, L. M., Philippar, U., Pinheiro, E. M., Burds, A. A., Bronson, R. T., Mori, S., Fässler, R., and Gertler, F. B. (2007) Ena/VASP Is required for neuritogenesis in the developing cortex. *Neuron* **56,** 441–455
3. Garvalov, B. K., Flynn, K. C., Neukirchen, D., Meyn, L., Teusch, N., Wu, X., Brakebusch, C., Bamburg, J. R., and Bradke, F. (2007) Cdc42 regulates cofilin during the establishment of neuronal polarity. *J. Neurosci.* **27,** 13117–13129
4. Strasser, G. A., Rahim, N. A., VanderWaal, K. E., Gertler, F. B., and Lanier, L. M. (2004) Arp2/3 is a negative regulator of growth cone translocation. *Neuron* **43,** 81–94
5. Bradke, F., and Dotti, C. G. (1999) The role of local actin instability in axon formation. *Science* **283,** 1931–1934
6. Sobue, K., Muramoto, Y., Fujita, M., and Kakiuchi, S. (1981) Purification of a calmodulin-binding protein from chicken gizzard that interacts with F-actin. *Proc. Natl. Acad. Sci. U.S.A.* **78,** 5652–5655
7. Sobue, K., and Sellers, J. R. (1991) Caldesmon, a novel regulatory protein in smooth muscle and nonmuscle actomyosin systems. *J. Biol. Chem.* **266,** 12115–12118
8. Mayanagi, T., and Sobue, K. (2011) Diversification of caldesmon-linked actin cytoskeleton in cell motility. *Cell. Adh. Migr.* **5,** 150–159
9. Sobue, K., Morimoto, K., Inui, M., Kanda, K., and Kakiuchi, S. (1982) *Biomed. Res.* **3,** 188–196
10. Ngai, P. K., and Walsh, M. P. (1984) Inhibition of smooth muscle actin-activated myosin Mg^{2+}-ATPase activity by caldesmon. *J. Biol. Chem.* **259,** 13656–13659
11. Sobue, K., Takahashi, K., and Wakabayashi, I. (1985) Caldesmon150 regulates the tropomyosin-enhanced actin-myosin interaction in gizzard smooth muscle. *Biochem. Biophys. Res. Commun.* **132,** 645–651
12. Ishikawa, R., Yamashiro, S., and Matsumura, F. (1989) Differential modulation of actin-severing activity of gelsolin by multiple isoforms of cultured rat cell tropomyosin. Potentiation of protective ability of tropomyosins by 83-kDa nonmuscle caldesmon. *J. Biol. Chem.* **264,** 7490–7497
13. Yamashiro, S., Chern, H., Yamakita, Y., and Matsumura, F. (2001) Mutant Caldesmon lacking cdc2 phosphorylation sites delays M-phase entry and inhibits cytokinesis. *Mol. Biol. Cell* **12,** 239–250
14. Fukumoto, K., Morita, T., Mayanagi, T., Tanokashira, D., Yoshida, T., Sakai, A., and Sobue, K. (2009) Detrimental effects of glucocorticoids on neuronal migration during brain development. *Mol. Psychiatry* **14,** 1119–1131
15. Sobue, K., and Fukumoto, K. (2010) Caldesmon, an actin-linked regulatory protein, comes across glucocorticoids. *Cell Adh. Migr.* **4,** 185–189
16. Kira, M., Tanaka, J., and Sobue, K. (1995) Caldesmon and low Mr isoform of tropomyosin are localized in neuronal growth cones. *J. Neurosci. Res.* **40,** 294–305
17. Tanaka, J., Watanabe, T., Nakamura, N., and Sobue, K. (1993) Morphological and biochemical analyses of contractile proteins (actin, myosin, caldesmon and tropomyosin) in normal and transformed cells. *J. Cell Sci.* **104,** 595–606
18. Jiang, M., and Chen, G. (2006) High Ca^{2+}-phosphate transfection efficiency in low-density neuronal cultures. *Nat. Protoc.* **1,** 695–700
19. Riedl, J., Crevenna, A. H., Kessenbrock, K., Yu, J. H., Neukirchen, D., Bista, M., Bradke, F., Jenne, D., Holak, T. A., Werb, Z., Sixt, M., and Wedlich-Soldner, R. (2008) Lifeact: a versatile marker to visualize F-actin. *Nat. Methods* **5,** 605–607
20. Morita, T., Mayanagi, T., Yoshio, T., and Sobue, K. (2007) Changes in the balance between caldesmon regulated by p21-activated kinases and the Arp2/3 complex govern podosome formation. *J. Biol. Chem.* **282,** 8454–8463
21. Ray, J., Peterson, D. A., Schinstine, M., and Gage, F. H. (1993) Proliferation, differentiation, and long-term culture of primary hippocampal neurons. *Proc. Natl. Acad. Sci. U.S.A.* **90,** 3602–3606
22. Velaz, L., Ingraham, R. H., and Chalovich, J. M. (1990) Dissociation of the effect of caldesmon on the ATPase activity and on the binding of smooth heavy meromyosin to actin by partial digestion of caldesmon. *J. Biol. Chem.* **265,** 2929–2934
23. Hemric, M. E., and Chalovich, J. M. (1988) Effect of caldesmon on the ATPase activity and the binding of smooth and skeletal myosin subfragments to actin. *J. Biol. Chem.* **263,** 1878–1885
24. Li, Y., Zhuang, S., Guo, H., Mabuchi, K., Lu, R. C., and Wang, C. A. (2000) The major myosin-binding site of caldesmon resides near its N-terminal extreme. *J. Biol. Chem.* **275,** 10989–10994
25. Kuhn, T. B., Meberg, P. J., Brown, M. D., Bernstein, B. W., Minamide, L. S., Jensen, J. R., Okada, K., Soda, E. A., and Bamburg, J. R. (2000) Regulating actin dynamics in neuronal growth cones by ADF/cofilin and rho family GTPases. *J. Neurobiol.* **44,** 126–144
26. Warren, K. S., Lin, J. L., Wamblodt, D. D., and Lin, J. J. (1994) Overexpression of human fibroblast caldesmon fragment containing actin-, Ca^{++}/calmodulin-, and tropomyosin-binding domains stabilizes endogenous tropomyosin and microfilaments. *J. Cell Biol.* **125,** 359–368
27. Hayashi, K., Fujio, Y., Kato, I., and Sobue, K. (1991) Structural and functional relationships between h- and l-caldesmons. *J. Biol. Chem.* **266,** 355–361
28. Li, Y., Lin, J. L., Reiter, R. S., Daniels, K., Soll, D. R., and Lin, J. J. (2004) Caldesmon mutant defective in Ca(2+)-calmodulin binding interferes with assembly of stress fibers and affects cell morphology, growth, and motility. *J. Cell Sci.* **117,** 3593–3604
29. Wang, Z., Jiang, H., Yang, Z. Q., and Chacko, S. (1997) Both N-terminal myosin-binding and C-terminal actin-binding sites on smooth muscle

caldesmon are required for caldesmon-mediated inhibition of actin filament velocity. *Proc. Natl. Acad. Sci. U.S.A.* **94,** 11899–11904

30. Chantler, P. D., and Wylie, S. R. (2003) Elucidation of the separate roles of myosins IIA and IIB during neurite outgrowth, adhesion and retraction. *IEE Proc. Nanobiotechnol.* **150,** 111–125
31. Turney, S. G., and Bridgman, P. C. (2005) Laminin stimulates and guides axonal outgrowth via growth cone myosin II activity. *Nat. Neurosci.* **8,** 717–719
32. Loudon, R. P., Silver, L. D., Yee, H. F., Jr., and Gallo, G. (2006) RhoA-kinase and myosin II are required for the maintenance of growth cone polarity and guidance by nerve growth factor. *J. Neurobiol.* **66,** 847–867
33. Rösner, H., Möller, W., Wassermann, T., Mihatsch, J., and Blum, M. (2007) Attenuation of actinomyosinII contractile activity in growth cones accelerates filopodia-guided and microtubule-based neurite elongation. *Brain Res.* **1176,** 1–10
34. Bridgman, P. C. (2009) Myosin motor proteins in the cell biology of axons and other neuronal compartments. *Results Probl. Cell Differ.* **48,** 91–105
35. Hur, E. M., Yang, I. H., Kim, D. H., Byun, J., Saijilafu, Xu, W. L., Nicovich, P. R., Cheong, R., Levchenko, A., Thakor, N., and Zhou, F. Q. (2011) Engineering neuronal growth cones to promote axon regeneration over inhibitory molecules. *Proc. Natl. Acad. Sci. U.S.A.* **108,** 5057–5062
36. Letourneau, P. C., Shattuck, T. A., and Ressler, A. H. (1987) "Pull" and "push" in neurite elongation: observations on the effects of different concentrations of cytochalasin B and taxol. *Cell Motil. Cytoskeleton* **8,** 193–209

Original Paper

Cerebrovascular Diseases

Cerebrovasc Dis 2012;33:354–361
DOI: 10.1159/000335836

Received: August 7, 2011
Accepted: December 12, 2011
Published online: March 14, 2012

Effect of Combination Therapy with the Angiotensin Receptor Blocker Losartan plus Hydrochlorothiazide on Brain Perfusion in Patients with both Hypertension and Cerebral Hemodynamic Impairment due to Symptomatic Chronic Major Cerebral Artery Steno-Occlusive Disease: A SPECT Study

Hiroaki Saura[a, b] Kuniaki Ogasawara[a, b] Taro Suzuki[a, b] Hiroki Kuroda[a, b] Takeshi Yamashita[a, b] Masakazu Kobayashi[a, b] Kazunori Terasaki[b] Akira Ogawa[a, b]

[a]Department of Neurosurgery and [b]Cyclotron Research Center, Iwate Medical University, Morioka, Japan

Key Words
Hypertension · Angiotensin receptor blocker · Hydrochlorothiazide · Cerebral blood flow · Cerebrovascular reactivity

Abstract
Background: While the combination of an angiotensin receptor blocker with thiazide diuretics produces a clinically beneficial reduction in blood pressure in patients who otherwise only partially respond to monotherapy with an angiotensin receptor blocker, blood pressure-lowering therapy with combination antihypertensive drug regimens in patients with cerebral hemodynamic impairment may adversely affect cerebral hemodynamics. The purpose of the present exploratory study was to determine whether blood pressure-lowering therapy with the combination of the angiotensin receptor blocker losartan plus hydrochlorothiazide (LPH) worsens brain perfusion in patients with both hypertension and cerebral hemodynamic impairment due to symptomatic chronic major cerebral artery steno-occlusive disease. ***Methods:*** Patients with losartan-resistant hypertension and reduced cerebrovascular reactivity (CVR) to acetazolamide due to symptomatic chronic internal carotid artery (ICA) or middle cerebral artery (MCA) steno-occlusive disease were prospectively entered into the present study and received 50 mg/day of losartan plus 12.5 mg/day of hydrochlorothiazideat 14 weeks after the last ischemic event. Cerebral blood flow (CBF) and CVR were measured before and 12 weeks after initiating LPH using N-isopropyl-*p*-[^{123}I]-iodoamphetamine single-photon emission computed tomography (SPECT). A region of interest (ROI) was automatically placed in the MCA territory on each SPECT image using a three-dimensional stereotactic ROI template. ***Results:*** None of the 18 patients who participated in the study experienced any new neurological symptoms or adverse effects related to antihypertensive drugs. Systolic ($p < 0.001$) and diastolic ($p < 0.001$) blood pressures were significantly reduced after the administration of LPH, with average reductions of 11 mm Hg in systolic blood pressure and 10 mm Hg

KARGER

Fax +41 61 306 12 34
E-Mail karger@karger.ch
www.karger.com

1015–9770/12/0334–0354$38.00/0

Accessible online at:
www.karger.com/ced

Kuniaki Ogasawara, MD
Department of Neurosurgery, Iwate Medical University
19-1 Uchimaru
Morioka 020-8505 (Japan)
Tel. +81 19 651 5111, E-Mail kuogasa@iwate-med.ac.jp

in diastolic blood pressure. While in the affected hemisphere CBF did not differ between measurements taken before and after the administration of LPH, CVR was significantly higher after the administration of LPH than before ($p = 0.007$) and was significantly improved in 5 of 18 patients. In the contralateral hemisphere, CBF and CVR did not differ between measurements taken before and after the administration of LPH. There were no patients who experienced a significant deterioration in CBF or CVR in the affected or contralateral hemisphere after the administration of LPH. ***Conclusions:*** Although the present study was exploratory and its results were preliminary due to the small sample size, the current data suggest that blood pressure-lowering therapy with LPH apparently does not result in worsening of cerebral hemodynamics in patients with both hypertension and cerebral hemodynamic impairment due to symptomatic chronic ICA or MCA steno-occlusive disease.

Introduction

When the target blood pressure of patients with hypertension is not achieved with one antihypertensive drug, multidrug therapy should be considered [1]. In fact, multidrug therapy often produces greater blood pressure reduction at lower doses of the component agents [1].

Angiotensin receptor blockers inhibit vascular tone maintained by locally produced angiotensin II, resulting in vasodilatation of large cerebral arteries [2]. Further, pretreatment with an angiotensin receptor blocker protected hypertensive rats from brain ischemia by normalizing the cerebral blood flow (CBF) response [2], and a 4-week treatment course with this agent increased CBF in patients with a history of stroke [3]. In contrast, thiazide-type antihypertensive drugs induce diuresis, and oral long-term administration of these drugs may lead to dehydration and affect blood rheology. Treatment with hydrochlorothiazide decreases cardiac output by reducing extracellular fluid volume and plasma volume [4] and increases whole blood viscosity and hematocrit [5–8], which may reduce brain perfusion. However, the effect of combination therapy with an angiotensin receptor blocker plus a thiazide-type antihypertensive drug on brain perfusion remains unknown.

Among patients with symptomatic major cerebral artery occlusive disease, the subgroup of those with cerebral hemodynamic impairment is at increased risk of recurrent ischemic strokes [9]. Studies have demonstrated that patients with reduced cerebrovascular reactivity (CVR) to acetazolamide measured by single-photon emission computed tomography (SPECT) show an increased risk of a subsequent stroke [10, 11]. In patients with both hypertension and cerebral hemodynamic impairment, blood pressure-lowering therapy with an angiotensin receptor blocker plus a thiazide-type antihypertensive drug may adversely affect cerebral hemodynamics, facilitating the development of ischemic stroke.

The purpose of the present exploratory study was to determine whether blood pressure-lowering therapy with the combination of the angiotensin receptor blocker losartan plus hydrochlorothiazide (LPH) worsens brain perfusion in patients with both hypertension and cerebral hemodynamic impairment due to symptomatic chronic internal carotid (ICA) or middle cerebral artery (MCA) occlusion.

Methods

Patients

The study prospectively enrolled patients who satisfied the following criteria: age >20 years; carotid artery territory ischemic symptom within the last 2 months before presentation to our department; useful residual function (modified Rankin disability scale 0 or 1); unilateral or bilateral ICA or MCA atherosclerotic stenosis (≥70%) or occlusion on magnetic resonance angiography or angiography with arterial catheterization; losartan-resistant hypertension and moderately reduced CVR defined by criteria described below. Exclusion criteria were: pregnancy or breast-feeding; angina pectoris or myocardial infarction within 6 months before presentation to our department; congestive heart failure (New York Heart Association class 3/4); stenosis of the bilateral or unilateral renal arteries; serum creatinine >2.0 mg/dl, and aspartate aminotransferase >90 IU/l and/or alanine aminotransferase >80 IU/l.

A local ethics committee approved the study protocol. Written informed consent was obtained from all subjects prior to enrollment in the study.

Management and Medications

Upon the patient's presentation to our outpatient department, a physician or a nurse measured his/her blood pressure twice consecutively using the auscultatory method with a mercury sphygmomanometer while the patient was in the sitting position after a rest of at least 2 min. Blood pressure was defined as the average of the two measurements.

No antihypertensive drugs were given to patients within 8 weeks after the last cerebral ischemic event. When systolic or diastolic blood pressure 8 weeks after the last cerebral ischemic event was >140 or >90 mm Hg, respectively, patients received 25 mg/day of losartan; when the systolic or diastolic blood pressure at 2 weeks after initiating the administration of losartan was above the target value, patients received 50 mg/day of losartan; when the systolic or diastolic blood pressure at 4 weeks after initiating the dose escalation of losartan was still above the target value, pa-

tients were defined as having losartan-resistant hypertension and received 50 mg/day of losartan plus 12.5 mg/day of hydrochlorothiazide (LPH) (Preminent®).

During the study period, all patients received antiplatelet drugs such as aspirin (100 mg/day) or clopidogrel (75 mg/day).

Patients visited our outpatient clinic at 2-week intervals until 12 weeks after initiating the administration of LPH. At these visits, clinicians determined whether new neurological symptoms developed, and blood pressure was measured.

Measurement of Brain Perfusion Using SPECT

Brain perfusion was assessed using [^{123}I]N-isopropyl-*p*-iodoamphetamine (IMP) and SPECT. The IMP SPECT studies, including measurements at the resting state and with acetazolamide challenge, were performed as described previously [12]. Studies were performed twice: the day before initiating the administration of LPH and 3 months later. The CBF images were calculated according to the IMP autoradiography method [12, 13].

All SPECT images were transformed into the standard brain size and shape by linear and nonlinear transformation using SPM99 for anatomic standardization [14]. Thus, the brain images of all patients had the same anatomic format. Next, 318 constant regions of interest (ROIs) were automatically placed in both the cerebral and cerebellar hemispheres using a 3D stereotaxic ROI template [15]. The ROIs were grouped into 10 segments (callosomarginal, pericallosal, precentral, central, parietal, angular, temporal, posterior, hippocampus and cerebellum) in each hemisphere according to the arterial supply. Only 5 (precentral, central, parietal, angular and temporal) of these 10 segments were combined and defined as a ROI perfused by the MCA (fig. 1). The mean CBF value at the resting state and with an acetazolamide challenge in all pixels in the MCA ROI was calculated in each hemisphere. Then, CVR to acetazolamide was calculated as follows: CVR (%) = [(acetazolamide challenge CBF – resting CBF)/resting CBF]/100.

Using the same method, 10 normal subjects (8 men and 2 women; age, 35–65 years; mean age, 52.3 years) were studied twice at an interval of 3 months to obtain control values. For the first study, the means ± standard deviations (SDs) of CBF and CVR in the MCA ROI were 35.9 ± 4.4 ml/100 g/min and 36.8 ± 9.2%, respectively. When CVR in the MCA ROI of a patient was between the mean – 2SD (i.e. 18.4%) and the mean – 3SD (i.e. 9.2%) of the control value, it was rated as moderately reduced CVR; when CVR was ≤ the mean – 3SD, it was rated as severely reduced. Patients with moderately reduced CVR participated in the present study.

Differences between values obtained at the two studies (the second study – the first study) in the normal subjects were also calculated: 0.1 ± 4.5 ml/100 g/min for CBF and 1.1 ± 6.3% for CVR. When the difference between CBF or CVR obtained at the two studies (the second study – the first study) in a patient was ≥2SD above the mean control difference obtained from normal subjects (i.e. 9.1 ml/100 g/min for CBF; 13.7% for CVR), the patient was rated as having improved CBF or CVR, respectively; when the difference in a patient was ≤2SD below the mean control difference obtained from normal subjects (i.e. –8.9 ml/100 g/min for CBF; –11.5% for CVR), the patient was rated as having deteriorated CBF or CVR, respectively; when the difference in a patient was between 2SD above and below the mean control difference obtained from normal subjects, the patient was rated as having unchanged CBF or CVR, respectively.

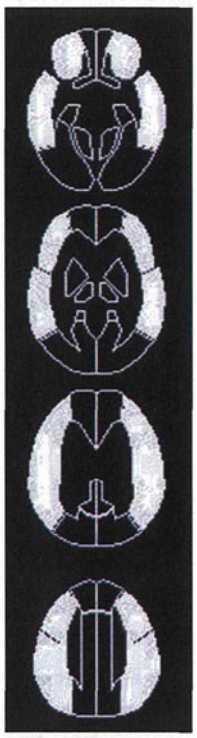

Fig. 1. Diagrams showing the ROIs of a three-dimensional stereotaxic ROI template. The white ROIs (precentral, central, parietal, angular, and temporal segments) indicate territories perfused by the bilateral MCAs.

Statistical Analysis

Because the present study was an exploratory trial, the required sample size could not be definitely estimated. Data are expressed as means ± SDs. Differences between blood pressure, CBF or CVR before and 12 weeks after initiating the administration of LPH were evaluated using the Wilcoxon signed-rank test. When there were patients with improved or deteriorated CBF or CVR, each variable was compared between patients with and without such a condition using the Mann-Whitney U test or Fisher's exact test. A multivariate statistical analysis of factors related to such a condition was also performed using a logistic regression model. In addition to variables with $p < 0.2$ in the univariate analyses, age and gender were selected for analysis in the final model. Statistical significance was set at the $p < 0.05$ level.

Results

During 30 months, 19 patients satisfied the inclusion criteria. Of these 19 patients, 1 had experienced angina pectoris within 6 months before presentation to our department and was excluded from the present study. Written informed consent was obtained from the remaining 18 patients, who ultimately entered into the present study. The characteristics of these 18 patients are summarized in table 1.

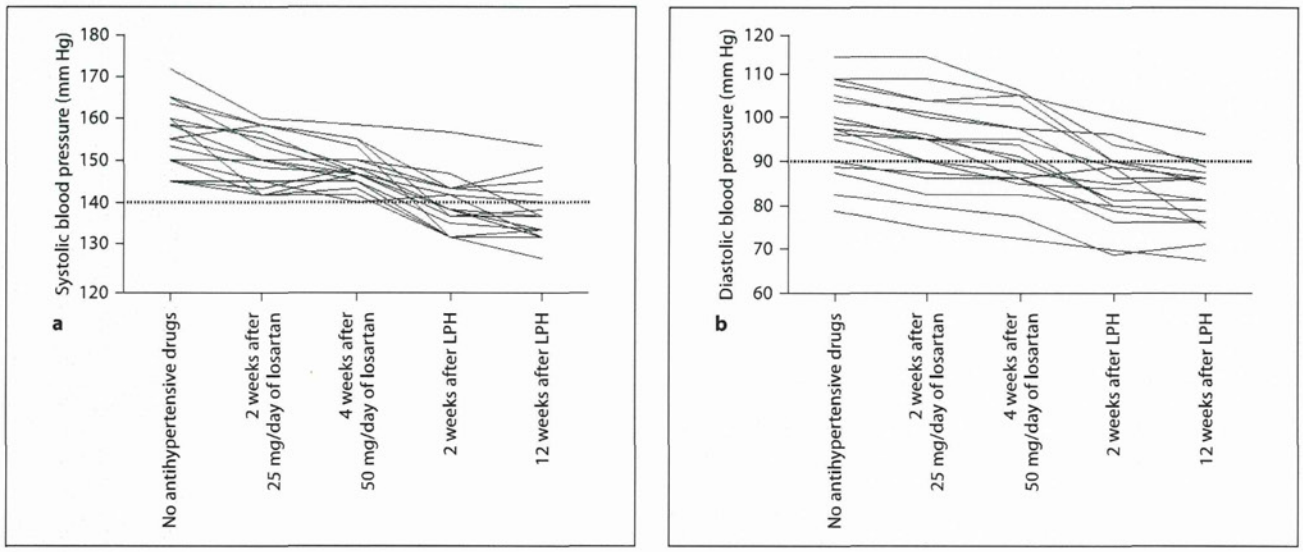

Fig. 2. Systolic (**a**) and diastolic (**b**) blood pressure values at each time point. Dashed horizontal line denotes a target value.

Table 1. Patient characteristics

Age	Gender	Body mass index	Current smoking	Excessive drinking	Diabetes mellitus	Dyslipidemia	Symptoms	Lesions on MRI	Lesions on angiography	Antiplatelet drug
67	M	26.9	yes	no	yes	yes	MCS	border zone INF	right ICA stn	CP
47	M	25.3	no	no	no	no	TIA	none	right MCA stn	AS
58	M	21.4	no	no	no	no	TIA	none	left ICA occl	CP
61	M	24.3	no	no	no	no	TIA	none	left ICA stn	AS
68	M	27.6	no	yes	no	yes	MCS	border zone INF	left ICA occl	CP
56	F	20.4	yes	no	yes	no	TIA	border zone INF	left MCA occl	AS
76	M	22.9	no	no	no	no	MCS	border zone INF	left ICA occl	CP
55	M	25.3	no	no	no	no	TIA	none	right MCA stn	AS
65	M	25.9	yes	no	yes	yes	MCS	border zone INF	left MCA occl	CP
48	M	27.3	no	no	no	no	TIA	border zone INF	right MCA occl	AS
57	M	23.6	no	no	no	yes	TIA	none	left ICA occl	AS
68	F	26.0	yes	no	no	no	MCS	border zone INF	left ICA occl	CP
55	F	22.7	no	no	no	no	TIA	none	left MCA occl	AS
65	M	22.2	no	no	no	no	TIA	none	right MCA occl	CP
48	M	26.4	no	no	yes	yes	TIA	none	left MCA occl	AS
72	M	22.5	yes	no	no	no	MCS	border zone INF	right ICA occl	CP
70	M	26.9	yes	no	no	yes	MCS	border zone INF	right ICA occl	AS
62	M	27.1	no	no	no	no	MCS	border zone INF	left ICA ocl	CP

Excessive drinking is defined as drinking alcohol >60 g/day. MRI = Magnetic resonance imaging; MCS = minor complete stroke; TIA = transient ischemic attack; INF = infarction; stn = stenosis; occl = occlusion; CP = clopidogrel; AS = aspirin.

All these 18 patients were followed up until 12 weeks after initiating the administration of LPH. All the patients also received antihypertensive drugs and underwent brain perfusion SPECT studies during the study period. None of the 18 patients experienced new neurological symptoms or adverse effects related to antihypertensive drugs.

Time courses of systolic and diastolic blood pressures for each patient are shown in figure 2. Systolic ($p < 0.001$)

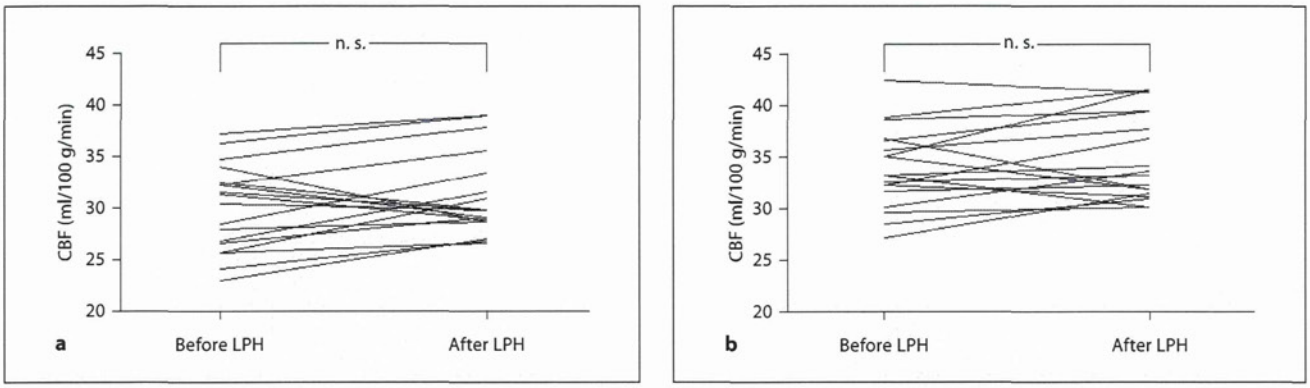

Fig. 3. Change in CBF in the affected (**a**) and contralateral (**b**) MCA territories before and after initiating the administration of LPH.

and diastolic ($p < 0.001$) blood pressures were significantly lower at 12 weeks after initiating the administration of LPH (138 ± 7 mm Hg for systolic blood pressure; 82 ± 7 mm Hg for diastolic blood pressure) than before the administration of LPH (149 ± 5 mm Hg for systolic blood pressure; 92 ± 10 mm Hg for diastolic blood pressure), respectively. Differences between values before and after the administration of LPH (values after administration – values before administration) ranged from 5 to 18 mm Hg for systolic blood pressure (11 ± 4 mm Hg) and from 2 to 18 mm Hg for diastolic blood pressure (10 ± 5 mm Hg).

CBF did not differ between measurements taken before and after the administration of LPH in the affected hemisphere (30.0 ± 4.2 ml/100 g/min before administration; 31.1 ± 4.1 ml/100 g/min after administration) or in the contralateral hemisphere (33.9 ± 3.9 ml/100 g/min before administration; 35.0 ± 4.3 ml/100 g/min after administration) (fig. 3). When based on differences between CBF before and after the administration of LPH, all patients studied were rated as having unchanged CBF in the affected and contralateral hemispheres.

While CVR in the affected hemisphere was significantly higher after the administration of LPH (23.6 ± 12.0%) than before (14.5 ± 2.3%) ($p = 0.007$), CVR in the contralateral hemisphere did not differ between these two measurements (40.0 ± 11.1% before administration; 41.7 ± 10.2% after administration) (fig. 4). When based on differences between CVR before and after the administration of LPH, in the affected hemisphere, 5 and 13 patients were rated as having improved and unchanged CVR, respectively. In the contralateral hemisphere, all patients were rated as having unchanged CVR. None of the patients were rated as having deteriorated CVR in the affected or contralateral hemisphere.

The results of the univariate analysis of factors related to improved CVR in the affected hemisphere are summarized in table 2. None of the variables, including blood pressure difference, were significantly associated with improved CVR. The following confounders were also adopted in the logistic regression model for the multivariate analysis: age, gender and site of lesion on angiography. The analysis revealed that none of the variables were significantly associated with improved CVR (table 2).

Figure 5 shows brain perfusion SPECT images in the resting state and with acetazolamide challenge before and 12 weeks after initiating the administration of LPH in patient 3.

Discussion

The present exploratory study suggests that blood pressure-lowering therapy with LPH does apparently not result in worsening of cerebral hemodynamics in patients with both hypertension and cerebral hemodynamic impairment due to symptomatic chronic ICA or MCA steno-occlusive disease.

Losartan is the first nonpeptide angiotensin II receptor antagonist studied in large clinical trials of patients with hypertension and diabetic nephropathy or left-ventricular hypertrophy [16, 17]. LPH produces a clinically beneficial reduction in blood pressure in patients who otherwise only partially respond to losartan monotherapy [18]. In the present study, systolic and diastolic blood pressures were significantly lowered by administration of

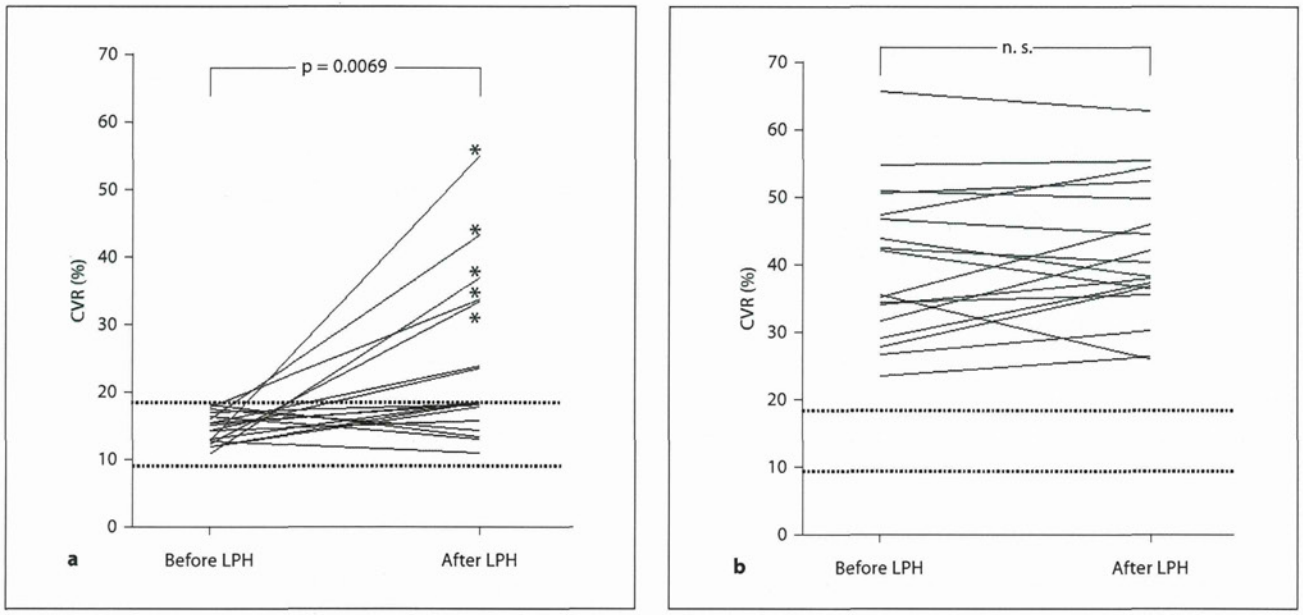

Fig. 4. Change in CVR to acetazolamide in the affected (**a**) and contralateral (**b**) MCA territories before and after initiating the administration of LPH. Upper and lower dashed horizontal lines denote mean –2SD and mean –3SD of CBF obtained in healthy volunteers, respectively. Asterisk denotes patients rated as having improved CVR.

Table 2. Factors related to improved CVR in the affected hemisphere

Factors	Improved CVR		p	
	yes (n = 5)	no (n = 13)	univariate analysis	multiple logistic regression analysis
Mean age ± SD, years	62.6 ± 5.7	60.4 ± 9.6	0.587	0.995
Male gender	5 (100%)	10 (76.9%)	0.522	0.997
Mean body mass index ± SD	24.6 ± 2.3	24.7 ± 2.3	0.882	
Current smoking	2 (40.0%)	4 (30.8%)	>0.999	
Excessive drinking	0	1 (7.7%)	>0.999	
Diabetes mellitus	1 (20.0%)	3 (23.1%)	>0.999	
Dyslipidemia	3 (60.0%)	3 (23.1%)	0.268	
Only TIA	3 (60.0%)	7 (53.8%)	>0.999	
Border zone INF	2 (40.0%)	8 (61.5%)	0.608	
ICA steno-occlusive disease	5 (100%)	6 (46.2%)	0.101	0.607
Clopidogrel	2 (40.0%)	7 (53.8%)	>0.999	
Mean difference in systolic blood pressure ± SD, mm Hg	11.8 ± 3.6	10.7 ± 4.5	0.553	
Mean difference in diastolic blood pressure ± SD, mm Hg	9.8 ± 3.9	9.8 ± 5.2	0.804	

Excessive drinking is defined as drinking alcohol >60 g/day. TIA = Transient ischemic attack; INF = infarction.